RANDOM SILVER NANOWIRE NETWORK EMBEDDED AZO TRANSPARENT AND CONDUCTING FILMS

by

Fen Qin

B.S., East China University of science and technology, 2013

Submitted to the Graduate Faculty of

Swanson School of Engineering in partial fulfillment

of the requirements for the degree of

Master of Science

University of Pittsburgh

2016

UNIVERSITY OF PITTSBURGH

SWANSON SCHOOL OF ENGINEERING

This thesis was presented

by

Fen Qin

It was defended on

March 30, 2016

and approved by

Jung-Kun Lee, PhD, Associate Professor

Department of Mechanical Engineering and Materials Science

Saidi Wissam, PhD, Associate Professor

Department of Mechanical Engineering and Materials Science

Nettleship Ian, PhD, Associate Professor

Department of Mechanical Engineering and Materials Science

Thesis Advisor: Jung-Kun Lee, PhD, Associate Professor

RANDOM SILVER NANOWIRE NETWORK EMBEDDED AZO TRANSPARENT AND CONDUCTING FILMS

Fen Qin, M.S

University of Pittsburgh, 2016

In this thesis, silver nanowire (Ag NW) networks are embedded into aluminum doped zinc oxide (AZO) to prepare transparent and conducting (TC) films. The nanowires are of different length and diameters according to various reaction times and temperatures. The electrical properties, such as carrier concentration, carrier mobility and resistivity are studied using Van Der Pauw Hall measurement. The optical properties such as Mie scattering, Transmission and Haze are studied from both experimental and simulating results. The best Ag NW embedded TC film shows a low resistivity ~3.6 $\times 10^{-4} \Omega \cdot$cm with transmission ~ 85%. The theory of percolation is used to explain the connectivity effect of nanowires on the conductivity and transparency of TC films. Moreover, the optical improvement by adding silver nanoparticles is also discussed and showed. Small nanoparticles with diameter ~20nm can reduce the haze causing by silver nanowire networks.

TABLE OF CONTENTS

LIST OF TABLES

LIST OF FIGURES

ACKNOWEDGMENT

I would like to express my deepest appreciation to all those who helped and supported me to finish this study. A special and sincere gratitude I give to my advisor Prof. Jung-Kun Lee for his patience, motivation and immense knowledge. His guidance helped me a lot throughout my study.

Besides my advisor, I also want to thank my lab partners: Dr. Gillsan Han, Dr. Po-Shun Huang, Dr. Hyunwoo Shim and Ziye Xiong, Salim Caiskan for sharing decent and valuable experiences with me.

My thanks also go to the rest of my committee: Prof. Saidi and Prof. Nettleship who gave me encouragement and insightful suggestions.

1.0 INTRODUCTION

Transparent conducting oxides, abbreviated as TCOs, are optical transparent and electrical conductive thin film materials, can be widely used as opto-electrical apparatus such as OLEDs, solar cell, photovoltaics and displays.[2] As we all know, glass fibers absorb almost no light, thus are nearly 100% transparent materials. However, they are electrical insulators. On the other hand, material like silicon and other compound semiconductors are electrical conductive but wavelength dependent optical resistors. TCOs highly combine these two advantages and become the intermediate with both high transparency and conductivity.

Intrinsic oxides are usually insulators. However, doping with tiny amount impurities, the concentration of free electrons would increase dramatically, which leads to a lower resistivity. [2] In the past 100 years, TCO thin film has been greatly developed. The first TCO material was reported by Badeker [#] in 1907. According to Badeker's paper, CdO was prepared by oxidizing a sputtering film of Cd in the vacuum. However, the CdO is no longer used due to its toxicity. From 1957 to 2015, indium-tin-oxide (ITO), tin oxide (SnO_2), indium oxide (In_2O_3) and zinc oxide (ZnO) and their derivatives are the most interested by the scientists. [2]

Among different kinds of TCOs, indium-tin-oxide (ITO) is used as TCO in almost all the flat panel displays (FPDs), and other applications due to its excellent transparency and conductivity. [3] Generally, ITO has a 3×10^{-4} ohm-cm low resistivity and a visible transmittance of around 85%. This combination of electrical and optical properties has become

the “Gold Standard” for TCOs. The best ITO films reported by Fraser & Cook showed an even lower resistivity round 1.77 x 10^{-4} ohm-cm.[2]

However, the price of tin is about 5 times than that of base metal such as Zinc, Copper and Lead. Moreover, ITO is too brittle to be fabricated into application which requires high flexibility. As a result, our motivation in this study is to create a base metal based TCOs which has a competitive conductivity and transmittance compared with ITO. ZnO then became a perfect candidate. Aluminum doped zinc oxide exhibit both high transmittance and high conductivity. AZO film using sputtering method shows a 1 x 10^{-4} ohm-cm. But in this study, sol-gel method was used due to its simple process and low cost.[5]

On the other hand, nano-scale conductive metal, such as silver nanowires, is promising to improve the conductivity of TCOs and not affect the transparency a lot. In this study, we try to embed random silver nanowire networks into the AZO/ZnO conductive oxides to improve the conductivity of our thin films. Silver nanowire links well to each other and form a network, which can be a “highway” for the transfer of electrons. Silver thin films, with a thickness around 10nm, exhibit an carrier concentration around 10^{22} cm^{-3}, while a silver nanowire network embedded in AZO shows an carrier concentration round 5×10^{20} cm^{-3} but with a high transparency. Additionally, we add silver nanoparticles into nanowire networks to serve as decorations and improve the transmittance to some degrees. It has been reported that if nanoparticles attach on the surface of nanowires with certain gap, the haze causing by rough surfaces of silver nanowires can be reduced to some degree. [13]

2.0 BACKGROUND INFORMATION AND LITERATURE REVIEW

Transparent and conducting oxides (TCOs) are electrical conductive and optical transparent as well. Their absorption of visible light is close to zero and their conductivity is competitive with the conductors, which arouse the interests among the scientists.

2.1 TRANSPARENT AND CONDUCTING OXIDES

Transparent conducting oxides, abbreviated as TCOs, are optical transparent and electrical conductive thin film materials, which can be widely used as opto-electrical apparatus such as OLEDs, solar cell, photovoltaics and displays. In this chapter, a literature review of general TCOs and especially, ZnO-based TCOs are introduced.

2.1.1 TCOs development and review

The electrical conductivity and optical transparency are governed by the band gaps of materials. In metallic material, there exists a high density of free electrons sitting upper the Fermi energy, which leaving the transmission is due to the reaction with low energy photons. So, metal always shows a high conductivity but low transmittance. While in insulate materials, conductive band and valence band are separated by the band gap, which enable the transmission for each

wavelength lower than the band gap. Thus the transparency for insulators is always higher. Transparent conducting oxides compromise these two good properties and are optical transparent and electrical conductive. This is the reason people have interests in the researches about TCOs.

Transparent and conducting oxides (TCOs) usually refer to the materials with a structure like A_xB_y:D, where A is metal; B is non-metal oxygen-related part and D is dopant. The most popular A are tin, indium, zinc and the derivatives of their compounds.[2] Figure 2.1 shows the performance and development of these popular TCOs in the past several decades. And the derivatives, such as indium tin oxide (ITO) and aluminum doped zinc oxide (ZnO: Al), have low resistivity around $1\times10^{-4}\Omega$cm and high transmittance around 85%. In this study, these two important TCOs are emphasized to be discussed.

Table 2.1 TCOs and their dopants

TCO	*Dopant*
SnO2	Sb, As, Nb
ZnO	Al, In, Ge, Ti, Zr, Mg, As
In2O3	Sn, Mo, W, Zr, Mg, Nb
CdO	In, Sn
NiO	Li
Cr2O3	Mg, N

In the Table.2.1, it is learnt that all the dopant should have a reasonable valence so that an effective donor could be created if the origin metallic ion is replaced.

Figure 2.1 shows the development of resistivity in the past several decades. In the past 50 years, the process of making TCOs and the doping of intrinsic TCO materials have been developed and studied.

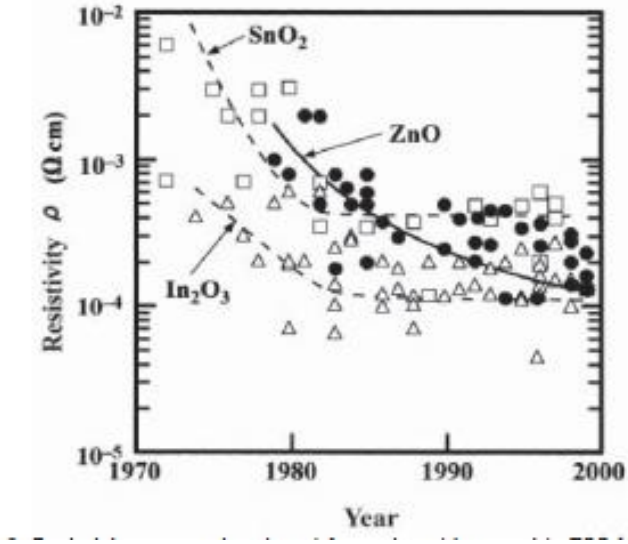

Figure 2.1. Resistivity development of TCOs (A: Sn, In, Zn) with years

2.1.2 Indium tin oxide (ITO)

Indium tin oxide (ITO), a mixture of around 90wt.% indium oxide (In_2O_3) and 10wt.% tin oxide (SnO_2), becomes one of the most important conductive transparent oxides in the past several decades. In today's industry, almost all the flat panels and touch panels use ITO as their transparent and conducting parts. The optimal tin concentration is necessary for low resistivity of ITOs. [3][12][22] Usually, the tin oxide is around 10 wt.%, but the amount can be slightly changed due to different purposes and different productions. Table 2.2 lists different kinds of ITO produced by different deposition techniques. The best ITO exhibits the resistivity as low as

$2\times10^{-4}\Omega$cm and a high transmission around 85%. This combination of electrical and optical properties has become the "Gold standard" for good TCOs for several decades.

Table 2.2. Optical and electrical properties of ITO summary

Deposition technique	Thickness (nm)	Hall mobility μH(sm2V-1s-1)	Carrier concentration (cm-3)	Resistivity (Ωcm)	Transmittance (%)
r.f. sputtering	700	35	6×10^{20}	3×10^{-4}	90
r.f. sputtering	500	12	12×10^{20}	4×10^{-4}	95
r.f.sputtering	400	25	3×10^{20}	8×10^{-4}	-
Magnetron sputtering	800	26	6×10^{20}	4×10^{-4}	85
d.c sputtering	100	35	9×10^{20}	2×10^{-4}	85
Reactive evaporation	250	30	5×10^{20}	4×10^{-4}	91
Ion beam sputtering	60	26	2×10^{20}	12×10^{-4}	-

The mobility is enhanced because the crystallinity of thin films using higher temperature. And the band gaps of ITO range from 3.5eV to 4.06eV, which is wider than the visible radiation and is the reason of high transparency of ITOs. [2] With Sn dopant, the carrier concentration increases as a result, the absorption limit shifts from the ultraviolent radiation into shorter wavelength areas. Figure 2.2 shows the assuming band gap structure of undoped In_2O_3 and Sn doped In_2O_3. After doping, the Fermi level jumped into the conductive band, which enlarges the optical band gap.

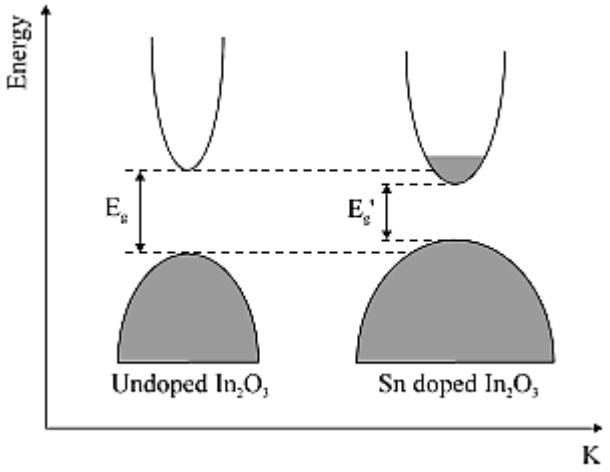

Figure 2.2. The assumption of the parabolic ITO band gap with and without the Sn doping[22]

2.1.3 ZnO: Al (AZO)

Besides the ITOs, another important TCOs is ZnO:Al (AZO). As introduced previously, AZO refers to Zinc oxide with aluminum as dopant. AZO can be made by various techniques, such as spray pyrolysis, sol gel method, chemical vapor deposition, d.c deposition and so on. Generally, ZnO produced by sol-gel solution has a high degree of crystal orientations, which decrease the possibility of the grain boundary (GB) scattering. As a result, the conductivity can be increased. Also the conductivity can be further improved by Al doping. ZnO is n-type semiconductor after doping with Al. The deposition methods, aluminum concentration, annealing conditions and other factors contribute to the difference of optical transparency and electrical conductivity of samples.

In the Figure 2.3, it shows that the resistivity and carrier has limitations with different doping amount. Although this limitation varies with different process, for example, for most sol-gel AZO, the limitation of Al doping is round 1at.%, this trend always exists. The reason lies

here is that Al located in the donor level should has the ability to be activated so that Al can increase the conductivity. Or, if the Al exceeds the limitations, the extra Al can never be activated. As a result, the carrier concentration would increase and the resistivity would not be decrease any more.

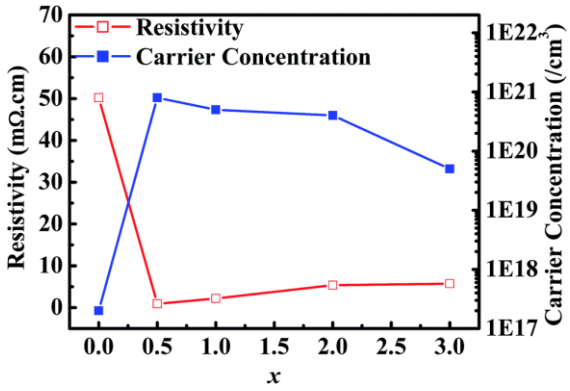

Figure 2.3 The resistivity and carrier concentration with different Al doping amount

For the transmittance of AZO, according to Figure2.4, all the films show a high transparency with transmittance around 90%.

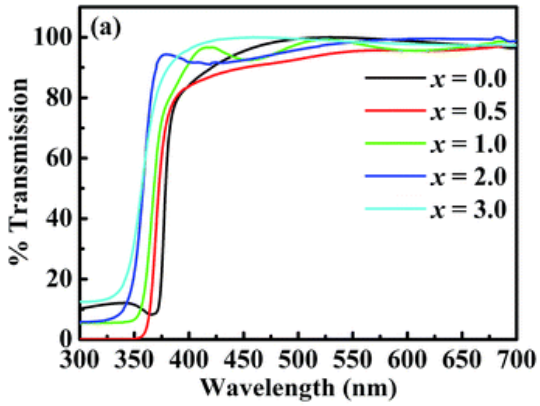

Figure 2.4 Transmittance of AZO with different Al doping amount

2.2 ELECTRICAL PROPERTY

2.2.1 Band gap theory

TCOs have wide band gaps, and their conductivity is in the range 10^2 – 10^6. As we all know, the semiconductor acts as insulators when it was in the original status. However, by doping, which is adding vacancies or interstitials into material, the conductivity will increase. Due to the EM theory, conductivity is mainly affected by electron density (n) and mobility (μ). The formula is built as following:

$$\mu = \frac{e\tau}{m_*} \tag{2.1}$$

τ here is the mean free path of electrons, m*is the effective mass. Since the band gap of TCOs is > 3 eV, it will be hard to thermally stimulate electrons into conduction band at room temperature (kT ~ 0.03 eV), which makes stoichiometric crystalline TCOs a good insulator in the room temperature.[3][4]

Many efforts have been denoted to build models or population mechanisms to explain the TCO characteristics. Some studies have shown that mobility has a close relation to the way the conduction band was populated.

2.2.2 ZnO and Al doped ZnO

Intrinsic defects in ZnO are due to the absence and displacement of lattice atoms. There are several kinds of defects: vacancies, interstitial defects and antisite defects. [1]

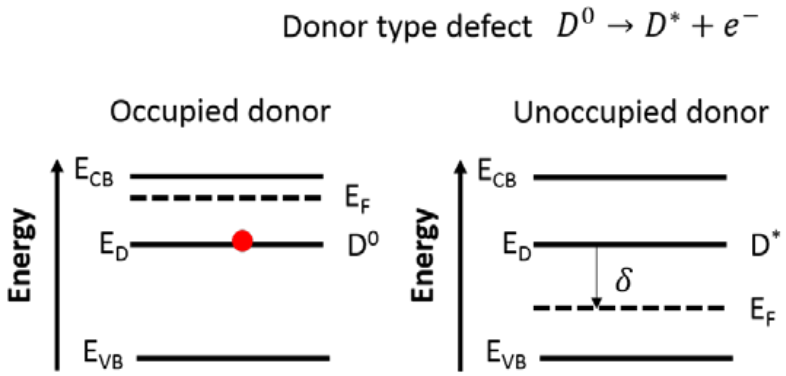

Figure 2.5. Band gap of donor type defect

For those intrinsic materials, impurity states that located near the conduction band are produced the metal interstitials or oxygen vacancies inside the material, which in turn makes the material conductive. The excess or donor electrons are stimulated into host conduction band at room temperature, though we can't tell which one plays a key role.

Carrier mobility is limited by Coulomb electrons and dopants interaction when the material is at high conducting electron density. So n and u are negatively related, conductivity σ can't be increased by simultaneously increasing n and u.

For Aluminum doped ZnO, the dopant increase the Fermi level, thus the electrons are easily to jump into the conductive band.

2.3 OPTICAL PROPERTY AND SIMULATOIN

2.3.1 Finite-difference time-domain (FDTD) simulation

Finite-difference time-domain (FDTD), also named as Yee's method, is a common method to simulate electromagnetic properties of materials. FDTD is classified as a grid-based differential time-domain numerical modeling method. It can cover a wide frequency range with a single simulation run, and can also simulate nonlinear materials properties in a natural way.

Among several electromagnetic simulation techniques, such as Method of moments (MOM), Fast multiple method (FMM), FDTD can solve Maxwell's equations in the time domain as well as in the frequency-domain. Since this is a time-domain method, the calculation of the electromagnetic field progresses at discrete steps in time. One advantage of the time domain method is that it can provide a broadband output from a single execution of the program. Furthermore, another advantage of FDTD is the excellent scaling performance of the method as the problem size grows.

In the FDTD simulation, both space and time are divided into discrete steps. For the space consideration, it is segmented into very small cubic cells, which is smaller than the length of wavelength. The electric fields are located on the edges of the cell and the magnetic fields are positioned on the faces as shown in Figure 2.6. This orientation of the fields is known as the Yee cell and is the basis for FDTD. For the time consideration, it is quantized into small steps. Each step represents the time required for the field to travel from one cell to the next. More cells connected to each other can form a 3-dimentional FDTD meshes.

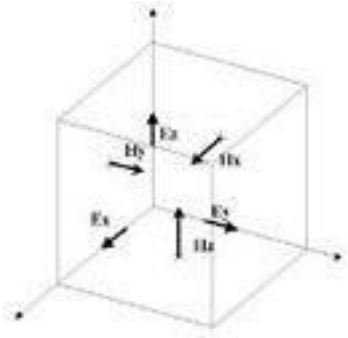

Figure 2.6. Yee cell

With 3-dimentional meshes linking to each other, materials such as conductor, dielectrics can be simply added by adjusting the equations for computing the fields at a certain location. For example of a conducting wire, the equations for the electric field can be simplified as zero because a perfect conducting materials' electric field is identically zero. By adding all the 3-dimentional end-to-end cells together, a conducting material can be defined. Using this method, a conducting wire is formed. Actually by this method, we can simulate any geometrical structure, such as the dielectric sphere shown in Figure 2.7

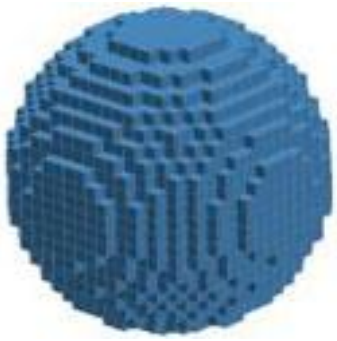

Figure 2.7. A dielectric sphere as meshed in an FDTD grid

The size of cell, the dimensions of the cubic boxes, is the most important constraint in any FDTD simulation since it determines not only the step size in time, but also the upper frequency limit for the calculation. Generally, the upper frequency limit is around ten cells per wavelength, while in practice the cell size will often be smaller than this in order to resolve dimensions and features of the structure to be simulated such as the thickness of a substrate or the length of a wire.

FDTD is a method capable of simulating a wide range of electric and magnetic materials. One of the basic materials is the free space. All the space is filled with free space until other materials is added into the free space.

Ideally conducting electric or magnetic materials are simulated by setting the values of electric or magnetic field to zero for each cell edges located in these materials. However, the conductor such as copper, whose equations for computing the fields are more complicated than ideal conductor, the calculation will take a longer time. Although, sometimes, if the number of meshes used to define a conductor is small, the difference in execution time will hardly be noticeable.

2.3.2 Rayleigh and Mie scattering

When an electromagnetic (EM) wave encounters a particle, the electron orbits around the particle will be perturbed periodically according to the frequency of the EM wave. This will lead to a displacement of the particle charge and generate a so called induced dipole moment.The induced dipole moment in turn generates EM wave. Those new EM wave are mostly in the same frequency as the incident EM wave. This is called the Rayleigh scattering.[25]

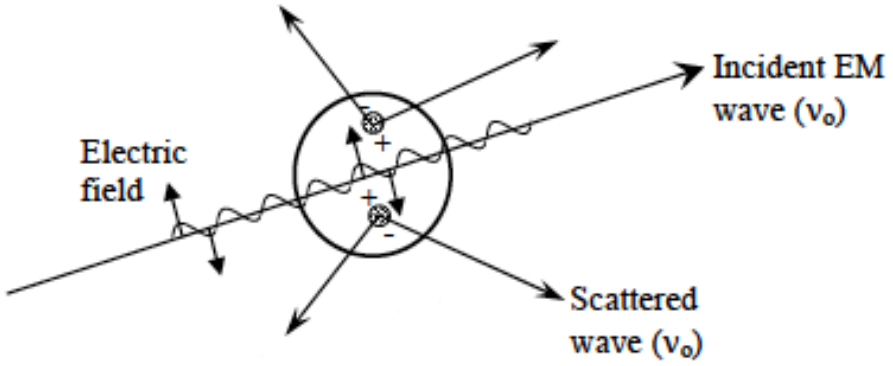

Figure 2.8. Light scattering by an induced dipole moment due to an incident EM wave [25]

There are two dominating light scatter theory, i.e. Rayleigh scattering and Mie scattering. Rayleigh scattering generally applies to small dielectric spherical particles, where Mie scattering applies to more spherical particles without size restriction. However, Mie scattering theory is much more complicated so Rayleigh scattering theory is preferred when it is applicable.

Mie scattering, also known as the Lorenz-Mie solution or the Lorenz-Mie-Debye solution, is usually used to simulate the scattering of an electromagnetic plane wave by a homogeneous sphere, and then also used to simulate the scattering of infinite cylinders or other structures. For scattering of tiny particles or molecules, which are smaller than 1/10 wavelength, is dominated by Rayleigh scattering, but for scattering of larger particles, whose size is larger than wavelength or comparable to wavelength, Mie scattering is dominated. Mie scattering leads to an antenna lobe. The larger the particles are, the shaper and more intense the lobe will be.

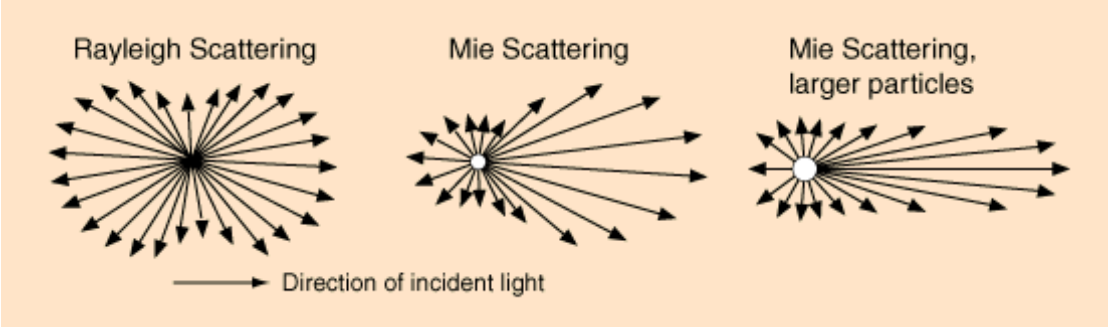

Figure 2.9. Two kinds of scattering

2.3.3 Surface plasmon resonance

Surface plasmon resonance is one of the unique spectroscopic features of metal nanoparticles (NPs). It affected the incident light's absorption and scattering. The mechanism of this phenomenon is to absorb a collective resonant oscillation of the free electrons in conductive band of metal. Figure 2.10 shows the electrons displaced from the original position under a resonant incident electric field.[28]

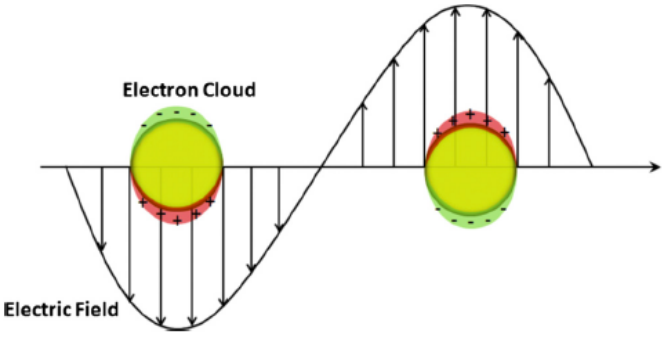

Figure 2.10. Schematic of surface plasmon resonance where the free electrons in the metal CB are driven into oscillation due to strong coupling of incident photons.

By surface plasmon resonance process, the electrons in the conductive band oscillate coherently. The loss of this coherence does not involve any energy redistribution such converting of heat, but solely the change in oscillating planes of electrons. The whole process can be viewed as a deactivation of the excited state. The energy dissipated by NPs can be acted like the emission of a photon. However, there exists another relatively higher efficiency process, called electron-electron relaxation, which reasonably explain the equilibrium of the excited electrons in NPs. The excited electrons can undergo collision with other electrons between nanoparticles, which brings a partition of energy. And finally this process would change the energy distribution from the highly non-thermal distribution.

A more direct way is to compare the absorption contour of cross section, shown as Fig.2.11. It is not hard to find that the silver particle increase the absorption near the surface and decay by the thickness of the Si.

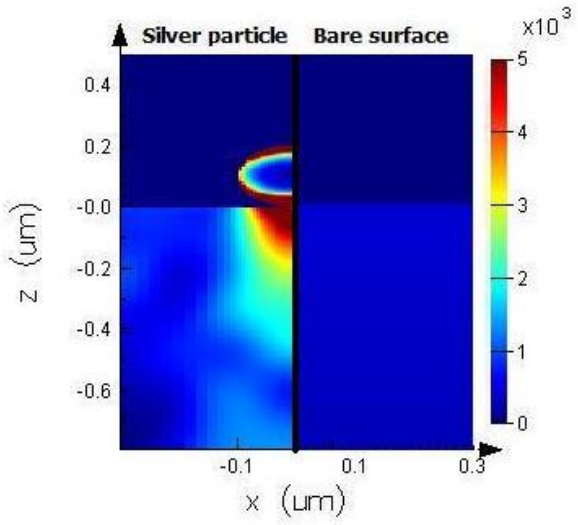

Figure 2.11. Absorption profile of nano-particle on Si and bare Si surface

By doping noble metal particles on the surface of semiconductor can effectively enhance the absorption near the surface. Additionally, different size of nanoparticles can absorb different range of light, which means that the non-uniform sizes of particles can obtain a broader absorption of light. And surface plasmon phenomenon can also happen under the surface since the solar cell structure is always a sandwich-like structure. Under surface plasmon may lead to more interesting results, however, the basic mechanism is the same.

2.3.4 Nanostructure shape and size effects

SIZE EFFECT: The optical properties of nanoparticles with different sizes vary a lot from each other. For example of gold nanoparticle, using Mie scattering theory to simulate the extinction, which is the sum of scattering and absorption by a spherical particle, it is clearly to see that the extinction peaks shift with different particles sizes and the scattering also differs. [17]

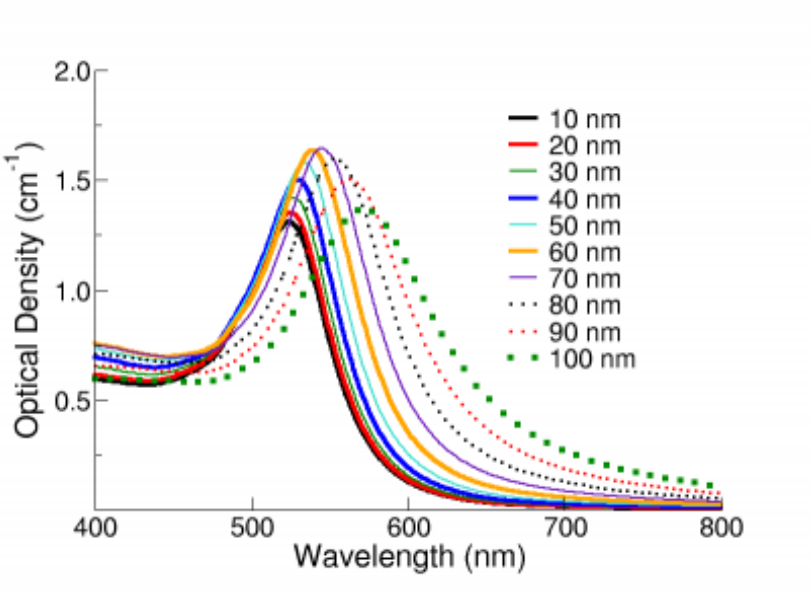

Figure 2.12. Optical density vs. wavelength with gold nanoparticle with different sizes

NANO-STRUCTURE: Additionally, nano-structures also have different impact on the optical properties. Here is an example of gold nanoshell and nanocage. For the solution, it is easy for us to judge by nude eyes. The color changes dramatically due to the sizes or shapes of nano-structure. [17]

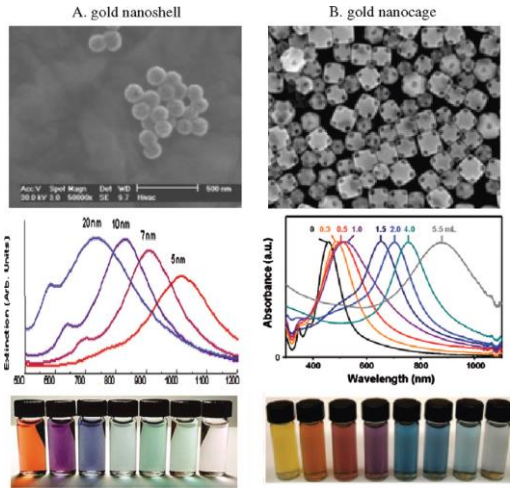

Figure 2.13. Different nano-structure gold and their color

CORE-SHELL STRUCTURE: Core-shell noble metallic particles can lead to a fano resonance, which is a process due to the coupling between surface plasmon resonance and the continuum of interband transitions of the others. Since the electromagnetic change and the thickness of the shell is hard to detect by TEM, the following part will still be explained by the simulation results, which is not the most realistic but more direct and theoretic results.

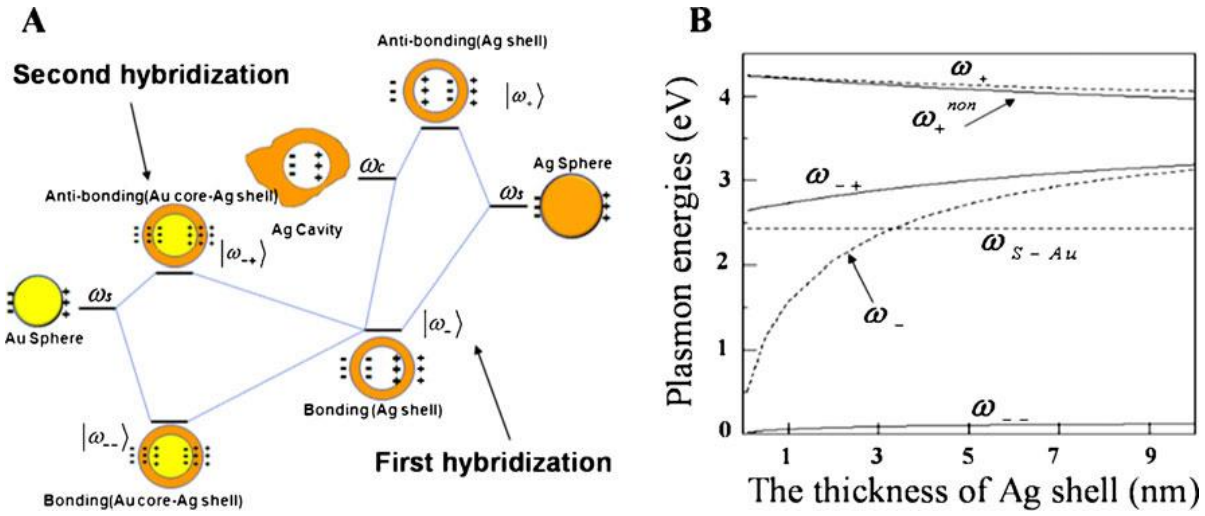

Figure 2.14. Plasmon hybridization theory: (a) Core-shell structure plasmon hybridization. (b) Calculated plasmon energy of the hybridized modes of the interacting system and the individual core models as a function of shell thickness.[4]

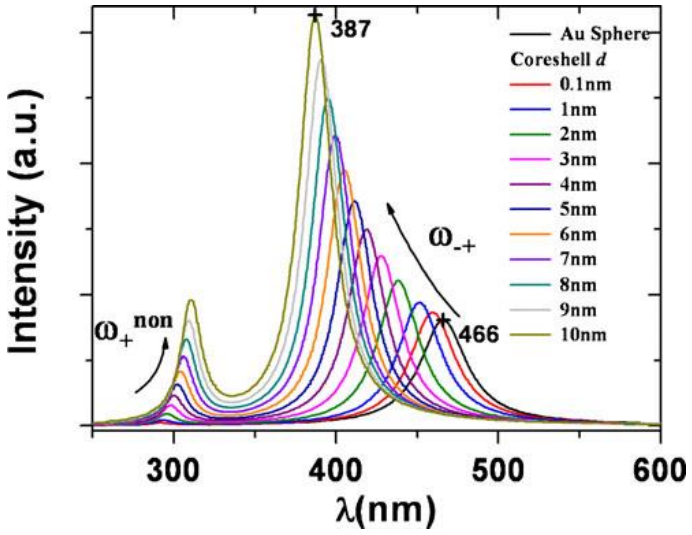

Figure 2.15. The plasmon absorption of the Au/Ag core-shell structure nanoparticles with different shell thickness, the radius of Au core is fixed at 15nm. [4]

From the Figure 2.14 and Figure 2.15, the plasmon absorption is obtained by the theory of plasmon hybridization theory and the intensity of absorption increases with the thickness of shell thickness.

Ag/Au core-shell structure is merely one of the basic models of core-shell structure. In fact, the shell can be any of the shapes such as cubic or cones. More and more solar cell engineers are now focus on the researches of nanoparticles and surface plasmons in order to increase the efficiency of both organic and inorganic solar cell.

2.4 LIQUID-PHASE SYNTHESIS

2.4.1 Co-precipitation methods

Many of the earliest synthesis of metal nanoparticles were completed by the co-precipitation methods. However, since the co-precipitation involves nucleation, coarsening and agglomeration simultaneously, the mechanisms of each step are still difficult to be fully understood. Two most basic methods, synthesis from aqueous solution and synthesis from non-aqueous solution, will be introduced.

Both metal precipitation process from aqueous solution or non-aqueous solution are the process of metal cation reduction. Among large amounts of reducing agents, one of the most common one is hydrogen gas. The other common reducing agents such as alkali metal borohydride, hydrazine hydrate and hydrazine dihydrochioride are widely used as solvate.

The equation for a typical reduction reaction:

$$Mn + + ne - \rightarrow M0 \qquad (2.2)$$

Correspondingly, the equation for the oxidation reaction:

$$X^m - ne^- \rightarrow X^{m-n} \quad (2.3)$$

As for hydrogen, H_2, the value E^0 is defined as zero at standard temperature and pressure, the electrochemical half-reaction of H_2:

$$2H^+ + 2e^- \rightarrow H_2 \qquad E^0=0.00V \quad (2.4)$$

That's the reason most of metal can be reduced to metallic ion in the atmosphere of H_2 with standard temperature and pressure and with adjustment of pH value.

For other solvate such as borohydrite ion, the electrochemical half-reaction can be expressed as:

$$B(OH)_3 + 7H^+ + 8e^- \leftrightarrow BH^{4-} + 3H_2O \qquad E^0=-0.481V \quad (2.5)$$

Thus, according to the theory, any metal which has a higher E^0 than the E^0 of the reducing agent, such as -0.841 for borohydride, and 0 for H_2^+, should have the ability of reduction with standard pressure and temperature at reasonable pH value. [24][29][30]

Table 2.3. Metal nanoparticle precipitated by aqueous solutions[30]

metal	*Original material*	*Reducing agent*	*stabilizer*	*avg diam(nm)*
Co	$Co(OAc)_2$	$N_2H_4 \bullet H_20$	None	~20
Ni	$NiCl_2$	$N_2H_4 \bullet H_20$ + NaOH	CTAB	10-36
Cu	$CuSO_4$	$N_2H_4 \bullet H_20$	SDS	~35
Ag	$AgNO_3$	Ascorbic acid	Daxad 19	15-26
Ag	$AgNO_3$	$NaBH_4$	TADDD	3-5
Pt	H_2PtCl_4	Potassium bitartrate	TDPC	<1.5
Au	$HAuCl_4$	Trisodium citrate	S3MP	10-50

Compared to synthesis from aqueous solution, the process of synthesis from non-aqueous solution is a valuable alternative, having advantages such as high crystallinity at relatively low temperature. For examples of gold nanoparticle synthesis methods used by Han et al., the gold was reduced in non-aqueous solutions. Formamide here served as the solvate and reducing agent as well. The reaction process was in the absence of oxygen. Poly(vinylpyrrolidone) (PVP) served as a stabilizer and it could also control the size of nanoparticles by adjusting the molar ratio of [PVP]/[Au]. [30]

2.4.2 Microwave methods

Microwave energy is a form of electromagnetic energy, which can influence the realm of molecular rotations. The energy released by microwaves is usually much higher than traditional oil bath synthesis, thus saves the time of synthesis and, on the other hand, creates more specific structures of materials, such as core-shell structure and hollow structure. [26]

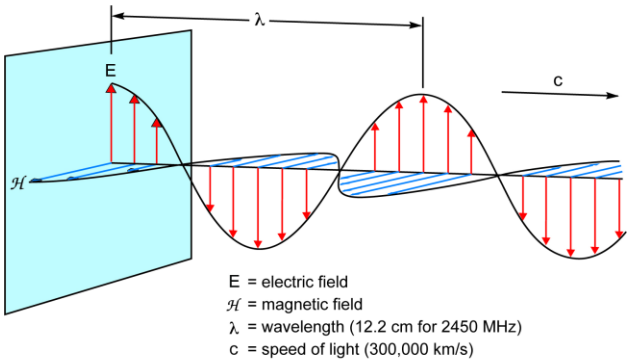

Figure 2.16. Electric and magnetic field in microwave

The electric field of a microwave heats matter through a phenomenon known as dielectric heating. As the electric field pass through the samples, the energy is transferred to molecules though the mechanisms of dipole rotation and ionic conduction. Unlike traditional chemical synthesis, the amount of solution taken part in microwave should be volumetrically and heated directly without the isolation by glass, which is largely transparent to microwave energy.

2.4.3 Sol-gel processing methods

Sol-gel is a chemical solution process describing when a sol, usually a colloidal or molecular suspension of solid particles of ions in a solvent transfers into a gel-like semi-rigid mass. The formation of the gel solution enables the particles or ions to join each other and link as a continuous network after the evaporation or removing of solvent from original sol. [30]

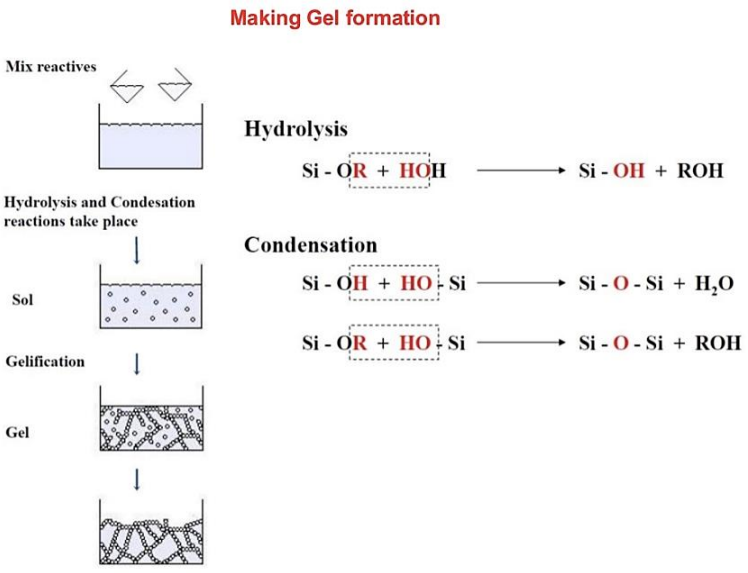

Figure 2.17. The process of sol-gel method [30]

The sol-gel process is interested because it is a cheap process and a relatively lower temperature process that enables a fine control on the chemical compositions of our products. Furthermore, even the amounts of dopants are small, such as inorganic dyes and rare earth metals. It is still possible that all the dopants are dispersed finely in the sol.

3.0 RESEARCH DESCRIPTION

3.1 HYPOTHESIS

The primary hypothesis of this study is that silver nanowire networks can improve the electrical properties of AZO matrix. Another hypothesis is that AZO, as a matrix, is able to collect the electrons and help to transfer the electrons into Ag NW networks. Then the electrons can transfer very well though the Ag NW networks. Finally, we also assume that, by adding silver nanoparticles into nanowire networks, the haze causing by the rough surfaces of nanowires can be reduced and the transmittance can be improved.

3.2 OBJECTIVES

In general, the main goal of this study is to experimentally discuss and explain the electrical and optical properties of Ag NW embedded AZO TC films with the assistance of optical simulation. Additionally, the effects on adding silver nanoparticle into nanowire networks is also discussed and explained.

3.3 TASKS

The first task of this study is to synthesize random silver nanowire networks with different diameters and lengths using polyol methods. The second task is making silver nanowire networks embedded AZO films and judge the performances of these films by both electrical conductivity and optical transparency. The third task is optical simulation to back up and explain the experimental results. Finally, the last task is to discuss how the silver nanoparticles can help to improve the performance of silver nanowire embedded AZO.

4.0 EXPERIMENTAL DETAILS

4.1 SILVER NANOWIRE/NANOPARTICLE SYNTHESIS

4.1.1 Silver nanowire

Solution A: Polyvinylpyrrolidone (PVP, M.W. ~ 55,000, 0.083g) was added into propylene glycol (PG) to get a viscous solution. PVP served as both protecting agent to limit the nanoparticle agglomeration and structure-directing agent because it could attach on {100} faces of silver, which lead to an anisotropic growth. Solution B: BMIM-Cl solution was prepared by dissolving 1-Butyl 3-methylimidazolium chloride (BMIM-Cl, $C_8H_{15}ClN_2$, 2.62g) into PG. BMIM-Cl prevent the silver nanowire from aggregation. Solution C: silver nitrite (0.085g) was dissolved in PG in order to get a homogenous silver nitrite solution. After solution A, B and C were ready, heated solution A at certain temperature for 5 min on a hot plate. And then 0.02g of solution B was dissolved in to solution A followed by further heating at certain temperature for 5 min. After heating, injected all the solution C into A/B mixture at a very slow injection rate (around 1mL/10min) using a pinhead. The totally reaction time for solution A/B/C mixture was differ from according to the table4-1. The transparent solution turned into orange color and eventually became turquoise color. Sufficient ethyl acetate was poured into turquoise solution A/B/C and obtained a brown mud-like precipitation of silver nanowire covered by PVP. The precipitation was cleaned by acetone for

several times in order to remove the PVP. In the end, brown precipitation was dissolved in to ethanol for further use.

Table 4.1. Conditions for nanowire growth

	#1	*#2*	*#3*	*#4*	*#5*
90°C	22h	26h			
100°C	6h	12h	24h	26h	
125°C	1h	2h	3h	4h	15h
150°C	0.5h	1h	1.5h	2.5h	3.5h

4.1.2 Silver nanoparticle

Polyvinylpyrrolidone (PVP, M.W. ~ 55,000, 2g) was added into 40mL ethylene glycol (EG) to get a viscous solution. After stirring at room temperature for about one hour, all the PVP dissolved. Then, silver nitrite (0.136g) was added into PVP/EG mixture. The mixture was heated on a hot plate at 120°C with 400rmp stirring rate. The whole reaction time was 30min. Initially transparent PVP/EG mixture changed to light yellow after adding the silver nitrite and then turned into a orange-like color and eventually became light brown due to the formation of nanoparticle sizes.

4.2 ZNO/AZO PREPARATION

4.2.1 ZnO sol-gel precursor

ZnO precursor was a mixture of zinc acetate dehydrate [Zn(CH3COO)2·2H2O], 2-methoxyethanol [CH3O(CH2)2OH], and monoethanolamine [MEA, NH2(CH2)2OH], which served as stabilizer to prevent unexpected $Zn(OH)_2$ precipitation . The molar ratio of [Zn]/[MEA] remained to 1. Both acetates (CH3COO) and amines (MEA) can help to get more cation Zn^{2+}. In the atmosphere of OH^-, Zn-MEA and Zn-acetate then developed into a network and became a viscous gel during the aging time (usually 24 h).

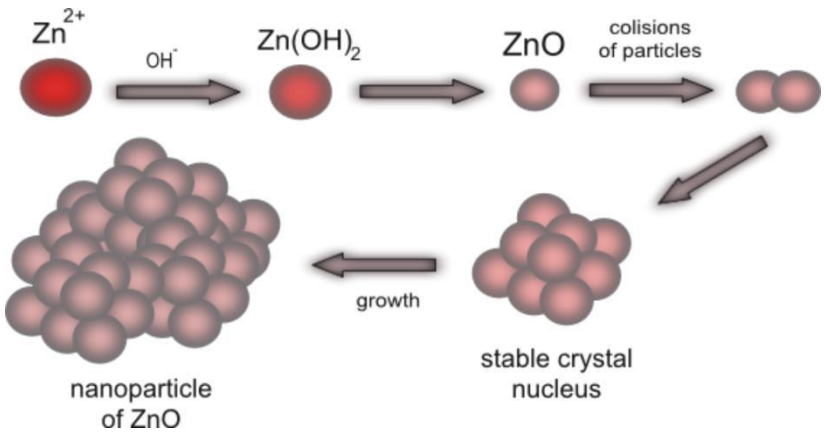

Figure 4.1. The growth mechanism of ZnO matrix

4.2.2 Aluminum doped ZnO (AZO)

The preparation of AZO precursors was similar to the one of ZnO but adding aluminum nitrite. The [Al]/[Zn] ratio had great impact on the properties of AZO. In this study, three different concentration of AZO, 1-3at.%, had been prepared and compared.

Aluminum is doped into pure ZnO solution so that it can tune the Fermi level and help to improve the conductivity. However, the doping limitation exists. It has been discussed that the maximum electrons or holes that coud be produced in a semiconductor has a limitation, which is a material property. [31] For our case, the Al doping limitation is around 1 at.%. After doping more aluminum in in ZnO, the conductivity just drops, as a result, the resistivity becomes larger.

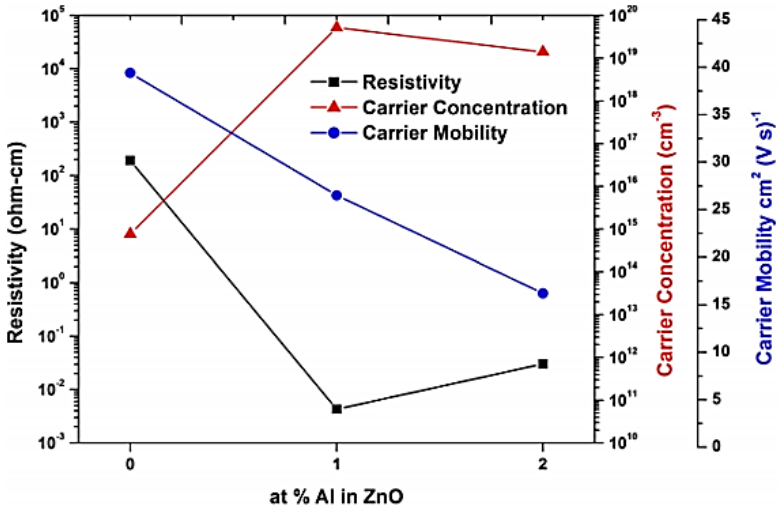

Figure 4.2. The resistivity, carrier concentration and carrier mobility for pure ZnO and AZO with different doping amount

4.3 CALIBRATION OF SILVER CONCENTRATION IN ZNO/AZO FILM

Because the amount of silver is critical in this study, in order to get a more accurate silver amount in different samples, XPS is used to do the calibration.

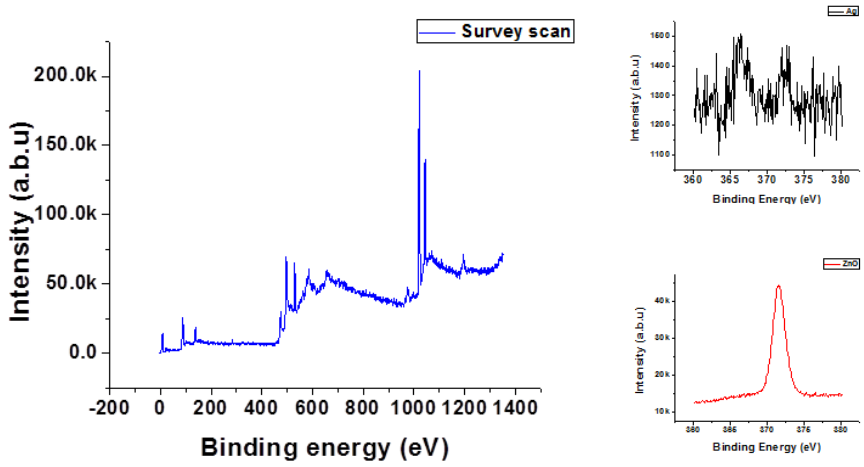

Figure 4.3. The survey scan, Ag scan and Zn scan from UPS

Table 4.2. Calibration of silver amount

Name	*Start BE*	*Peak BE*	*End BE*	*Height CPS*	*FWHM eV*	*Area (P) CPS.eV*	*Area (N) TPP-2M*	*Atomic %*
Ag3d	368.48	365.38	363.88	156.73	0.12	552.07	0	0.42
Zn2p	1023.58	1020.45	1017.48	59717.54	1.91	124254.37	0.04	99.58

The amounts of silver in later discussion are all based on this calibration. For example, if 10mL silver solution is put into 10mL ZnO solution, from the calibration, it shows the silver

amount equals to 1wt..%, then for 5mL silver mixes with 10mL ZnO solution, the silver amount should be 0.5 wt.%.

4.4 FABRICATION OF SILVER EMBEDDED AZO

To make a TCO using sol-gel method, we need to prepare the gel-solution, baking or annealing the sol-gel and make it condensed. In this study, the process is shown in Figure 4.4.

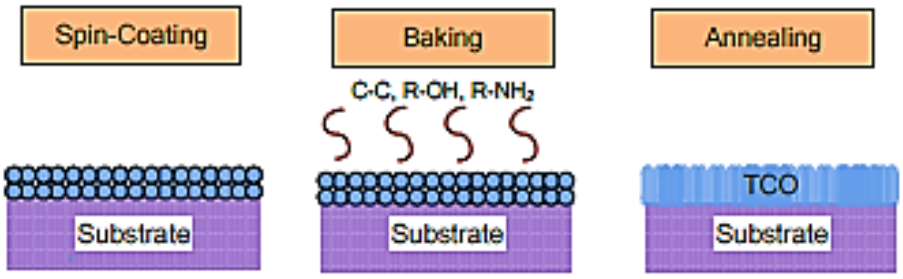

Figure 4.4. The process of TCO fabrication

4.4.1 Spin-coating and cross section thickness

In the process of spin-coating, as mentioned in chapter four, 3000rpm and 30seconds are applied. Due to the viscosity of sol-gel solution and the layers put on the substrate, samples can be varied with different thickness. From the equation below, the resistivity depends on the thickness of TCO layers. Thus, it is important to fix the thickness of our TCO layer for further comparison on electrical and optical properties. [32]

$$Rs = 4.53 \times V/I \quad \text{(eq 5.1)}$$

$$Rs = \text{resistivity/thickness (in cm)} \quad \text{(eq 5.2)}$$

From the cross section SEM image, the thickness of our TCO is round 200nm after seven times spin coating. For the samples with 100nm or lower, the thin film is not well connected, while for the samples with over than 200nm, the coating process takes too long time. Thus, finally, 200nm thickness is selected as the standard thickness for all the samples.

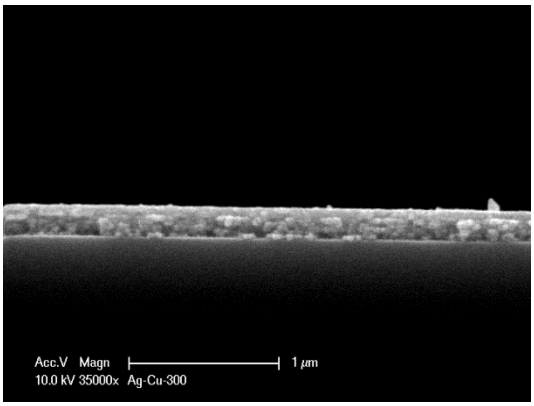

Figure 4.5. Cross section SEM images for the samples after spin coating for seven layers with 3000rpm and 30seconds

4.4.2 Baking temperature

After coating for each layer, baking is necessary to remove the MEA and other organic parts in the samples. The boiling temperature of Ethanolamine (MEA) is around 170°C, thus 200°C and 300°C are chosen as the baking temperatures. XPS of silver shows that 300°C would oxidize the silver nanowires on the surface thus reduce the conductivity, while 200°C is more suitable for removing MEA and keep silver nanowire from oxidization.

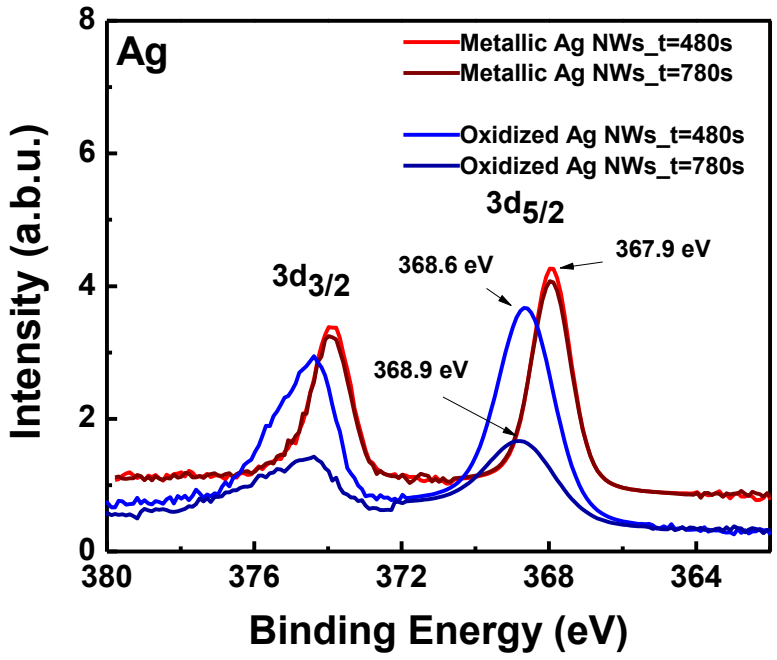

Figure 4.6. The XPS of silver scan for the samples with different baking temperatures

4.4.3 Annealing process

After spin-coating and baking, the samples are put in the tube furnace and annealed. The nitrogen is filled in the tube during the heating process while the forming gas, which consist of 95% nitrogen and 5% hydrogen, is filled during the cooling process in order to reducing the unexpected oxidization.

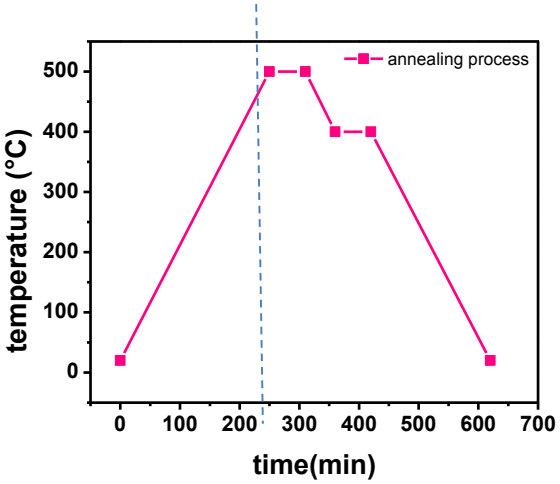

Figure 4.7. The annealing process

4.5 ULTRA-VIS SPECTROSCOPY

Since UV or visible radiation have interaction with the elements in specimens, electron transitions from lower energy states into higher states happen. Usually, from the electromagnetic spectrum, UV light locate in the region between 190~380nm, while visible light sit at a region from 380nm to 750nm. In this study, in order to learn about the scattering and haze caused by silver nanoparticles and nanowires, two methods have been used to measure the transmittance. [33]

4.5.1 Standard arrangement

For the most case, especially liquid specimens, standard arrangement is used to measure the transmission. By measuring a clear liquid (usually the pure solvate) as reference 100% transmittance, then it can be measured how much percentage of incident light has been

transmitted through the samples. Ideally, all the light scattered, reflected should be detected, however, if there exists the possibility of the transmitted beam deviating, overall transmittance is hard to be obtained.

4.5.2 Integrating spheres

Glass or thick films, which cause the problems like light scattering, reflection and bean distortion using standard arrangement, is more reasonable to be measured by integrating spheres. Integrated spheres compensate for all these problems, thus can obtain a more accurate results of transmittance. [18]

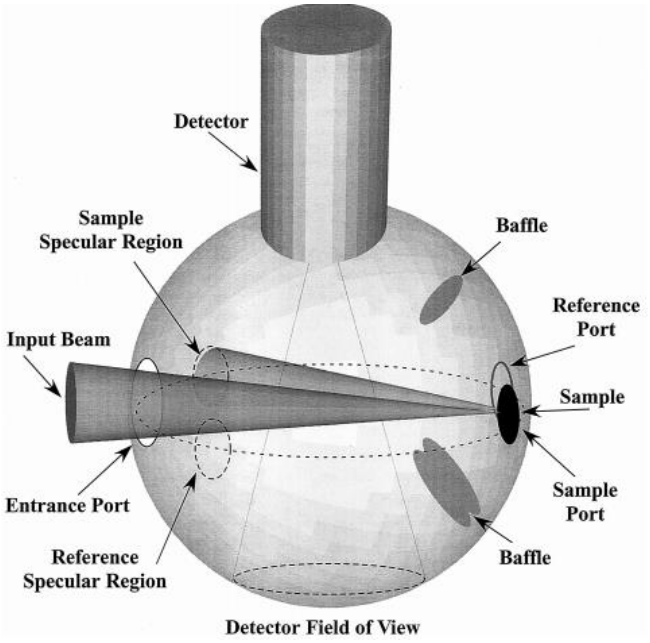

Figure 4.8. Diagram of sphere interior and arrangement of its elements

4.6 SCANNING ELECTRON MICROSCOPE

4.6.1 Scanning electron microscope (SEM)

By scanning our samples with a very focused beam of electron, SEM can get the images of samples. The atoms in samples show different interactions with electrons and help to obtain the information about both surface topography and composition of samples. Conventional SEM image is obtained by the secondary electrons, which can be emitted at the surface of specimen. Thus, usually, SEM can get relatively high-resolution surface images of samples.

4.6.2 Back-scattered electrons (BSE)

Reflected or back-scattered electrons(BSE) is another types of signals we can get from SEM. BSE refers to the beam electrons which are reflected by elastic scattering. Although the resolution of BSE images maybe worse than SEM image because BSE happens at a deeper locations of samples, BSE is widely used to analyze the distribution of different elements in specimen due to its dependence on atomic numbers.

4.6.3 Energy-dispersive X-ray spectroscopy

SEM can provide the information of composition by EDX analysis. Besides the secondary electrons and backscattered electrons, which are emitted during the SEM test, other important signals are also emitted from the specimen. When the incident beam hits the samples and create SE, on the other hand, thousands of holes are created simultaneously. If the holes located in the

inner shells of atoms, electrons from outer shells tend to drop into the inner shell in order to maintain the stability and minimize the energy of atoms. When the electrons move from a high-energy state outer shell into a low-energy state inner shell, there exists some energy loss in the atoms as the form of x-ray. Different elements have their unique energy gap between the outer and inner shells. Thus by detecting the x-ray emitted from different elements from different shell, we can get both the composition and even the shell, which lost the electrons and the shell, which replace the electrons as well.

4.7 X-RAY PHOTPELECTRON SPECTROSCOPY

4.7.1 X-ray photoelectron spectroscopy (XPS)

X-ray photoelectron spectroscopy (XPS) is a surface analysis technique that can be used to analyze the surface of samples or the surfaces after some treatment, such as ion beam etching to remove the contamination or oxidization thin layer on the surfaces of materials. The surface sensitivity enable the XPS to obtain a very high-resolution detection of electrons escaped from surface within less than 5nm into the vacuum of main chamber.

In this study, because the silver concentration and doping concentration are very limited, in order to get a more accurate calibration of silver amount mixed into the samples, XPS is used to do the surface chemistry analysis. Depth profile can be obtained by the multiple scanning of same positions with etching a certain thickness from the surface after each scanning.

4.7.2 Ultraviolet photoelectron spectroscopy (UPS)

Ultraviolet photoelectron spectroscopy is a technique measuring the kinetic energy spectra of photoelectrons created by samples when hit by the ultraviolet photons in order the get the information of valence band energy of the specimen. The principles are based on the Einstein's photoelectric law, showing as:

$$Ek=hv-I \tag{4.1}$$

h gives the Planck's constant, ν represents the frequency of the ionizing light, and I is the energy for the creation of an charged ion in the ground state or an excited state.

4.8 ATOMIC FORCE MICROSCOPE

4.8.1 Atomic force microscope (AFM)

Atomic force microscopy (AFM) was implemented to detect the thorough morphology of micro-nano scale droplets. In this study AFM was used to measure the topography of droplets, local roughness and cross-sectional profiles of the deposits.

There are two different detect mode in AFM detection, i.e. Tapping mode and Non-tapping mode. In tapping mode, the tip contacts with the sample surface, which as a result oscillates the cantilever and transfer back the electronic signal, while Non-tapping mode doesn't contaminate the sample but it produces much lower signal. Because a precise resonant frequency was needed in this experiment, tapping mode was used.

5.0 RESULTS AND DISCUSSION

This chapter describes how the embedded random silver nanowire networks in aluminum zinc oxide (AZO) or in Zinc oxide (ZnO) influence the electrical and optical properties. SEM images are presented to show the dimensions of nanowires produced under different reaction times and reaction temperatures. Optical properties and electrical properties are discussed using both experiment data, such as sheet resistance, carrier concentration and transmittance and FDTD simulations. Then the Ag NW ZnO fabricated perovskite solar cell J-V curve is compared with the perovskite using purchased FTO. Finally, some improvements on transmittance are discussed.

5.1 LENGTH AND WIDRH CONTROL OF SILVER NANOWIRES

The growth of silver nanowire was completed under different temperatures and reaction times, which was shown in table 4.1. The lengths and widths of nanowire were observed through SEM images.

5.1.1 Silver nanowire growth mechanism

Silver nanowires in this study are produced using polyol method. Silver nitrate is reduced with PG with assistance of PVP. At very beginning, five-folded silver nanoparticles are presented as seeds for nanowire growth. Decahedra structure of nanoparticles is preferred due to its five high energy twin boundaries. After a sufficient reaction time, the yellow-ish nanoparticle solution turn into grey, which indicates nanoparticles start to grow into nanorods and eventually into nanowires. Additionally, the silver nanowire solution become lighter and lighter with the nanowires grow longer and thicker. Surfactant PVP tends to attach selectively on {100} faces, which enable silver to grow in single direction. PVP also serves as a stabilizer, however, in order to make sure that the interaction between PVP with {111} facets is much weaker than the interaction between PVP with {100} facets, MEA is introduced to help PVP as a stabilizer, because MEA prefers to absorb on the newly formed {100} facets thus can guide the growth of nanowires. Ideally, we can observe five straight edges and five smooth surfaces. [34]

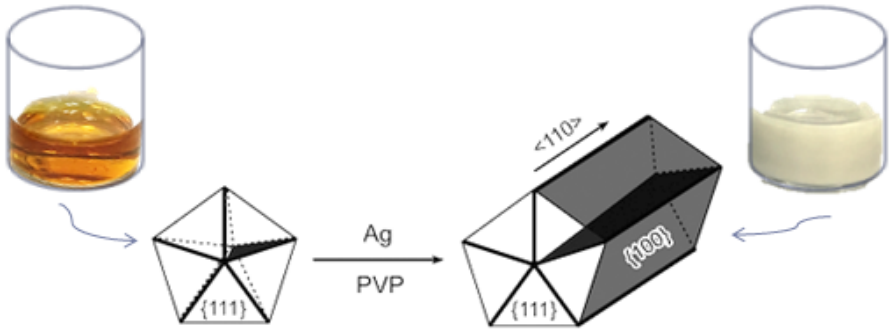

Figure 5.1. The growth mechanism of silver nanoparticle into silver nanowire

Furthermore, simulation on the extinction (absorption + scattering) shows, the growth of nanowire changes the extinction peak position and intensity as well.

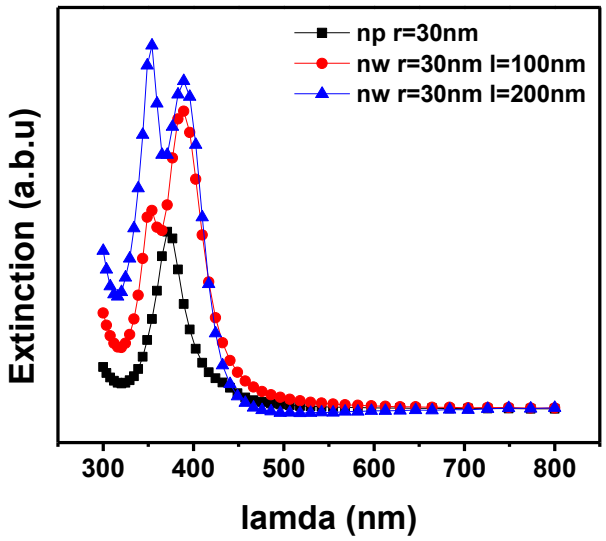

Figure 5.2. The simulation of extinction of nanoparticle (radius = 30nm), nanowire (radius = 30nm, length = 100nm) and nanowire (radius = 30nm, length =200nm)

5.1.2 Characterization of silver nanowire

Here, the SEM images for nanowires grown under 125°C with different reaction hours, 1hr, 3hr, 15hr, are shown respectively. From the SEM images, with longer reaction time, the nanowires are longer and fatter, while with shorter reaction time, the nanowires are shorter and thinner. Figure5.3 (a) and (b) show that when the reaction time is 1hr, the nanowire length ranges from 2 to 6 μm, and the width is around 40nm. Figure5.3 (c) and (d) show that when the reaction time is 3hr, the nanowire length ranges from 10 μm to 12μm, and the

width is around 60-70nm. Figure5.3 (e) and (f) show that when the reaction time is 15hr, the nanowire length is more than 15 μm, and the width is around 130-140nm.This trend is true for other nanowires when different temperature is applied.

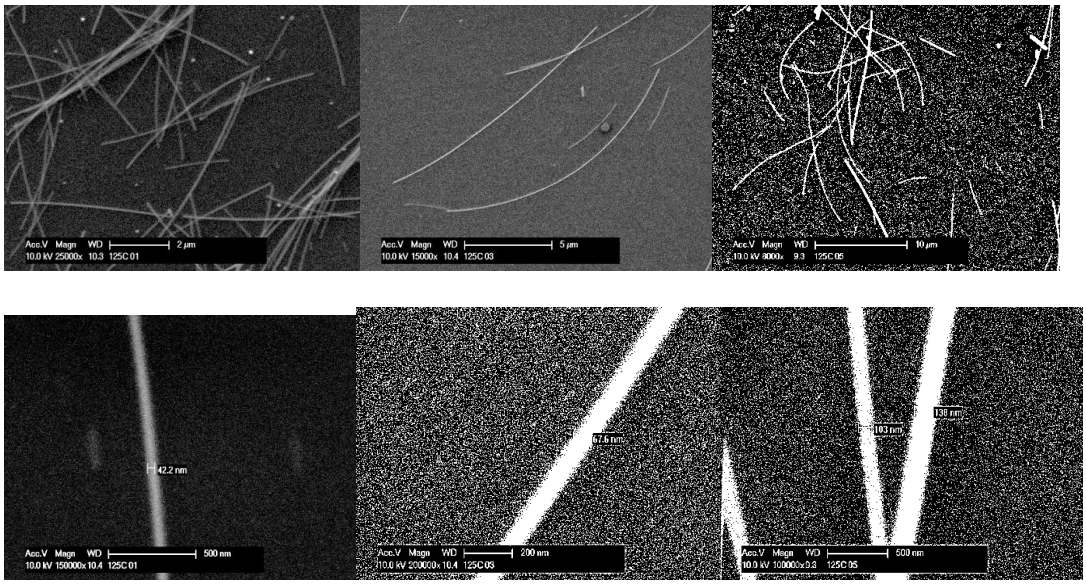

Figure 5.3. (a)(b) the length and width for silver nanowire grown under 125°C with 1hr; (a)(b) the length and width for silver nanowire grown under 125°C with 3hr; (a)(b) the length and width for silver nanowire grown under 125°C with 15hr

5.1.3 Silver nanowire dimension

After characterization of the nanowires with different conditions, in this part, the simple summary and comparison of length and width is presented and discussed.

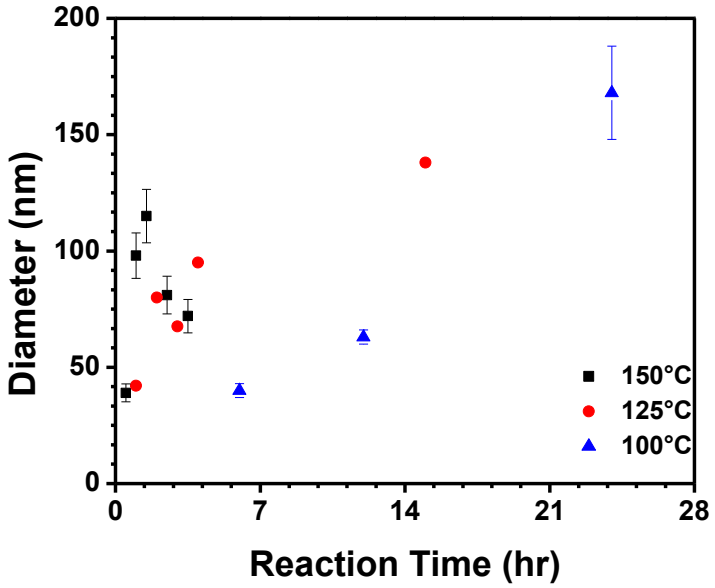

Figure 5.4. Silver nanowire diameters vs. reaction time for three different reaction temperature (100°C, 125°C, 150°C)

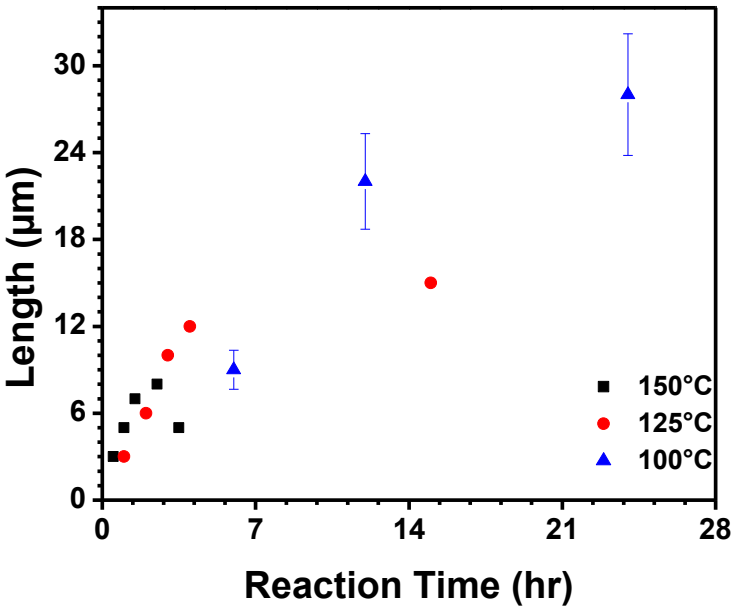

Figure 5.5. Silver nanowire length vs. reaction time for three different reaction temperature (100°C, 125°C, 150°C)

The plots comparing the lengths and widths of nanowires indicate that at lower temperature, and longer reaction time, the nanowires tend to grow longer and thicker. The possible reason is that at low temperature, the nucleation rate is relatively low, as a result, more silver nitrate reduces on the same seed, while at high temperature, such as 150°C the nucleation process is finished almost in 5-10 min, and there are more nucleation formed to nanowire growth. For higher temperature, the whole reaction process can be completed in couples of hours. Further reaction just leads to the melting or breaking of nanowires. For lower temperature, the nanowire keeps grow even after 24hr. The process takes a longer time.

5.2 OPTICAL AND ELECTRICAL PROPERTY -- EXPERIMENT

5.2.1 TCO fabrication

In the Figure 5.6 (b), it is not hard to tell that the nanowires are well protected from the high annealing temperature. All the nanowires are long and continuous. And in the Figure5.11(c), the intensity of silver marked as doted red line becomes stronger when the concentration of silver goes higher.

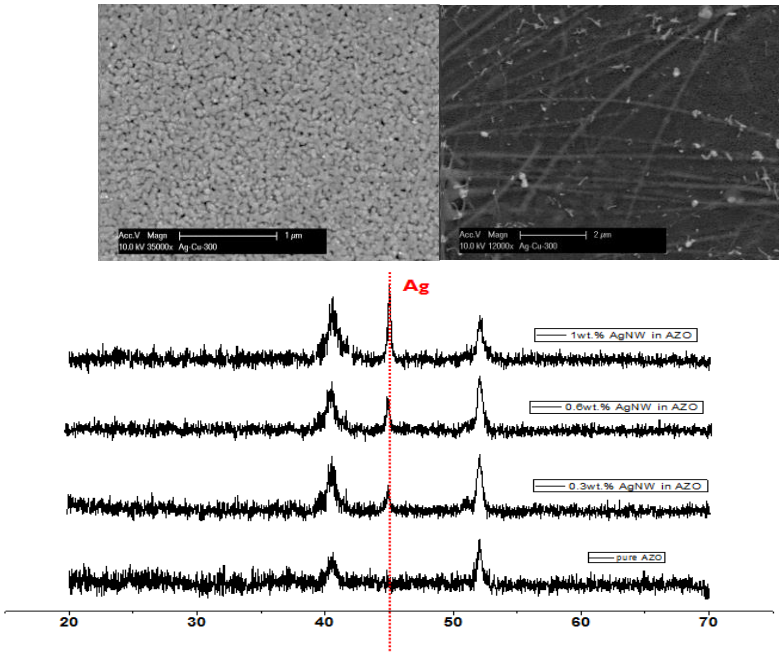

Figure 5.6. The samples after annealing (a) pure AZO; (b) silver nanowires embedded underneath the AZO; (c)XRD

5.2.2 Figure of merit

Figure of merit (FOM) is a standard figure that people try to compare and evaluate the optical and electrical properties for TCOS. Here, the "Gold standard" ITO sample, which marked as star dote line, is used to compare with the silver nanowires embedded AZO samples. From the FOM, we can see the silver nanowires with 60nm diameter and 28μm length has the highest transmittance and good conductivity. With same diameter, longer nanowire films have higher transmittance due to the smaller number of nanowires. With same length, thinner nanowires has higher transmittance.

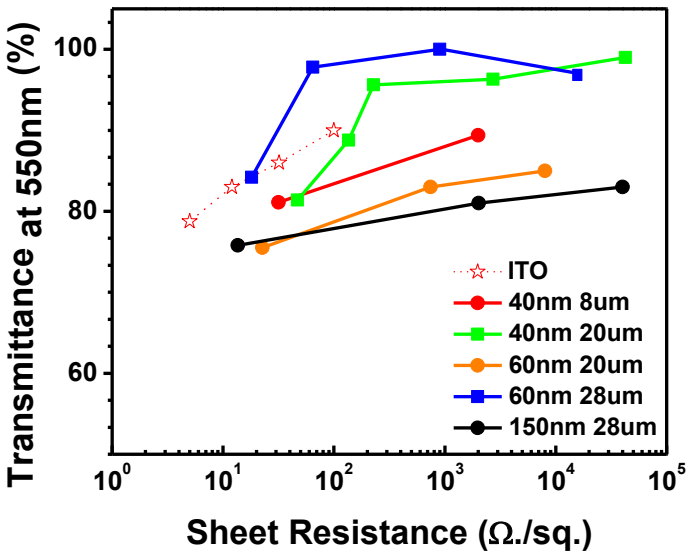

Figure 5.7. The FOM of silver nanowire embedded AZO compared with the ITO samples

5.2.3 Carrier transport

Aim to understand the carrier transport behavior in our samples, the Van Der Pauw measurement using Ecopia was used for further discussion.

Figure 5.8 is the Hall resistivity of silver nanowire embedded AZO films. As mentioned in Figure 5.7, the transmittance of blue line is over than 80%. Pure AZO matrix shows a semi-conductor behavior. Not like the pure AZO, after embedding the silver nanowire, the films perform more metallically. The resistivity decreases with lower temperature. Less electrons can be active as free electrons.

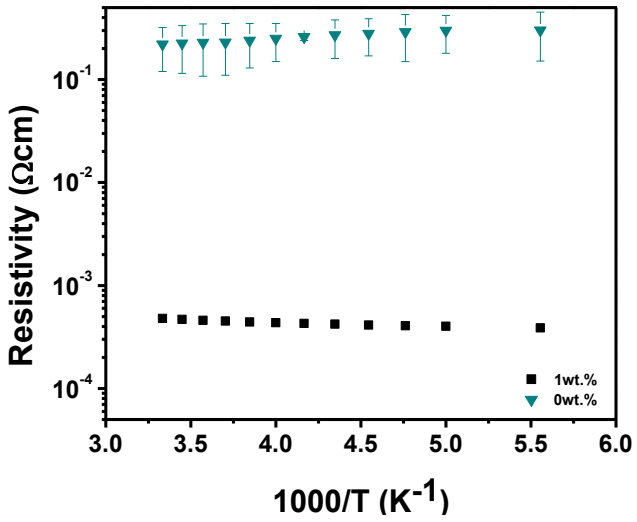

Figure 5.8. Temperature-dependence Hall resistivity of AZO/ Ag NW films

Furthermore, Figure 5.9 indicates that the carrier concentration and the carrier mobility can be enhanced by adding silver nanowires in the AZO matrix. Electrons can be donated by the silver nanowires, at the same time electrons can also transfer along the silver nanowires. Both the metallic and non-metallic behaviors contribute to the electrical performance in the films.

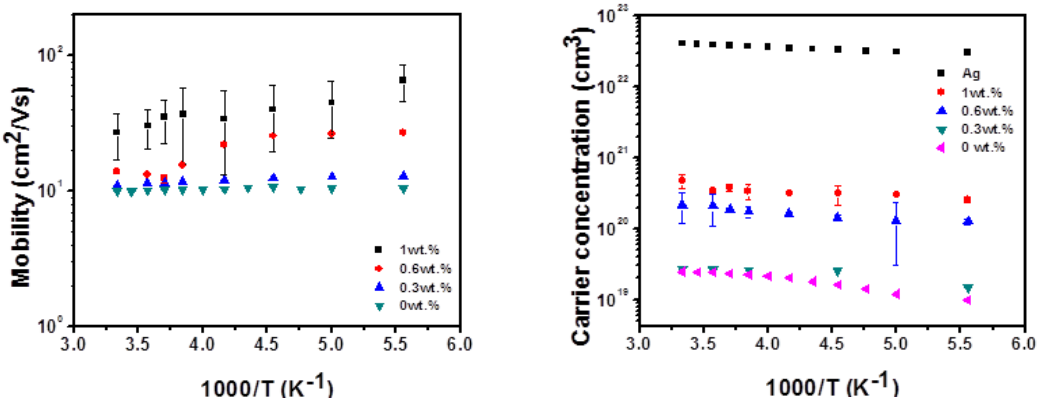

Figure 5.9. Temperature-dependence Hall mobility and carrier concentration

5.3 OPTICAL PROPERTY -- SIMULATION

As mentioned previously, the aim for this study is to combine the simulations with experimental results to discuss about the silver nanowire networks embedded TCOs. The next discussions are based on the FDTD simulation results accomplished by Lumerical. FDTD software. Within the scope of this study, the purposes of simulation part are the exploration of coverage ratio distributions, percolation limit distributions and nanoparticle decorated nanowire distributions on the transmission of the TCOs.

The randomness of silver nanowires can be observed experimentally using SEM. Figure 5.10(a)(b) show the ransom silver nanowire networks with low silver concentration and high silver concentration. Figure5.10 (c)(d) are top view and perspective view of our simulation models. The silver nanowires randomly disperse in the simulation box. Non-uniform meshes are set to simulate the curve edges for nanowires.

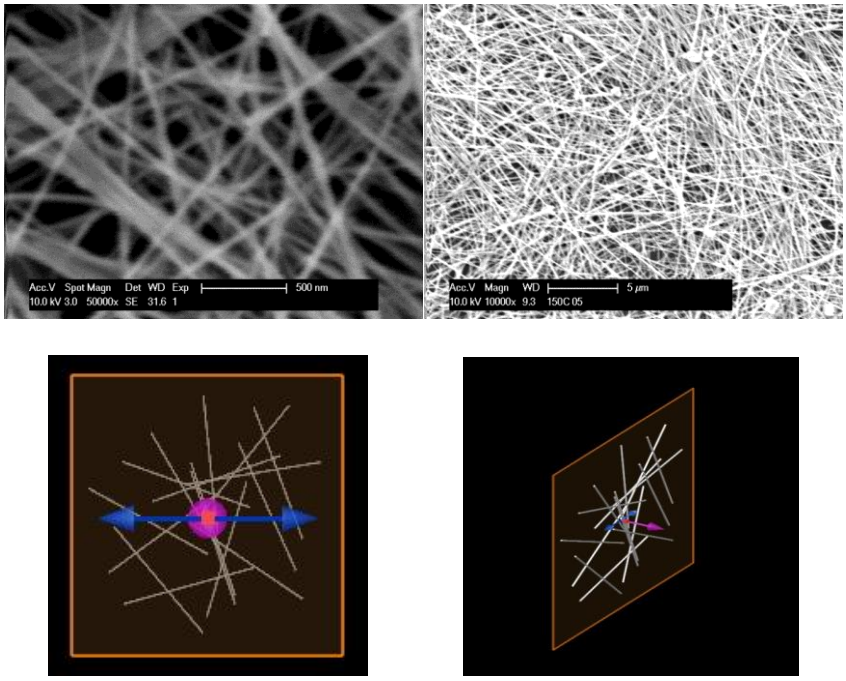

Figure 5.10. (a)(b) real silver nanowire networks with low and high concentration; (c)(d) the top view and 3-D perspective view of simulation box

5.3.1 Random silver nanowire networks

The random silver nanowire networks are created using Java in a 5×5μm frame with a fixed nanowire length 5μm, but different silver width from 30nm to 90nm and different coverage ratio from 0.1 to 0.5. Then the position information (x, y, z axis) and the rotation information (degree from each axis) are input into FDTD software to do the optical simulations.

The results of random silver networks are shown in the Figure 5.11. In doing so, we observed that larger number of nanowires is required for thinner diameter to meet the coverage ratio demand.

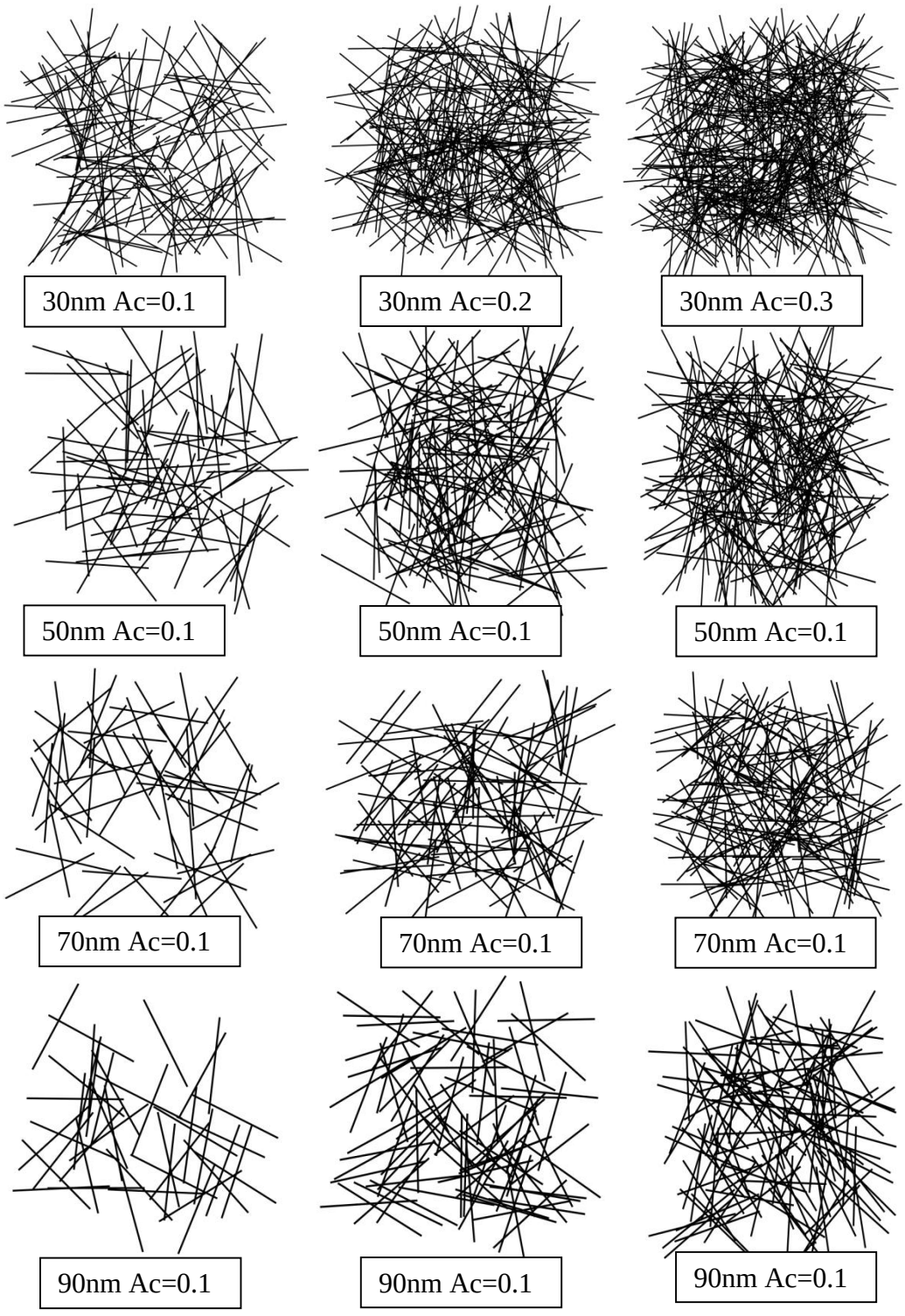

Figure 5.11. Silver nanowires with different diameters 30nm, 50nm, 70nm, 90nm and with different coverage ratio (Ac) 0.1, 0.2, 0.3, the length of nanowire fixes at 5μm

5.3.2 Transmission simulation with different coverage ratio

After importing all the parameters into FDTD, the silver nanowire networks are ready. Figure 5.12 are detailed the simplified models of our simulation. Silver nanowire network is under a plane-wave light source, whose wavelength sitting in the range of visible light from 300nm to 800nm. And all the transmission information is collected by a time-domain monitor.

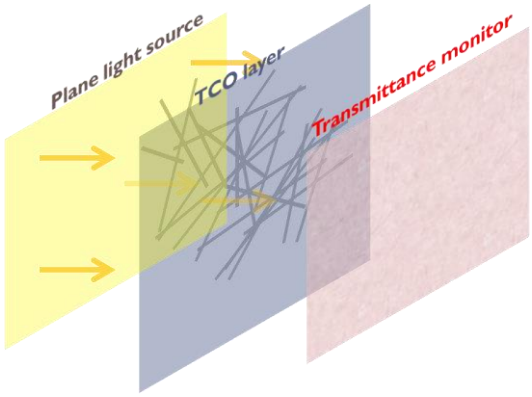

Figure 5.12. The simplified sketch of simulation model

The result of transmittance with various coverage area and different nanowire diameters are summarized in Figure 5.13. One of the key observations we can see from Figure 5.13 is that the transmittance of nanowires with larger diameter decays more quickly than the nanowires with smaller diameter. And the transmittance shows a linear relation with the coverage ratio regardless the length of nanowires. That meets the experimental transmittance results. If the nanowires are well connected, which means the concentration of silver is over the percolation limit. Thinner nanowires created a network with higher transmittance than the thicker nanowire network with similar resistivity.

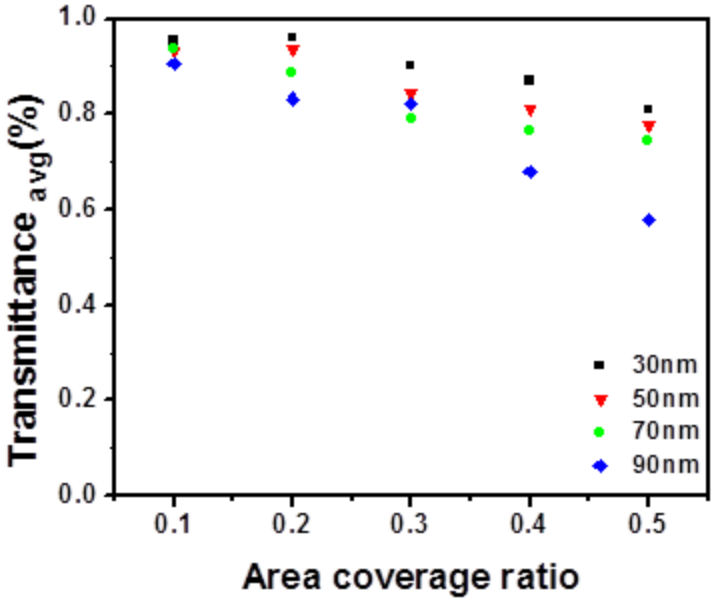

Figure 5.13. The transmittance vs. coverage ratio with different nanowire diameters

5.3.3 Transmittance at the percolation limit

In this section, a gentle introduction of percolation followed by the transmission simulation at the percolation limit is showed and discussed in order to better evaluate the effect of silver nanowire diameter effect on transmission of TCOs.

Percolation can be defined as the pathways through a material. In our case, the electrons transfer along the silver nanowire network in TCO film is fundamentally derived from percolation. There are several ways to express the percolation limit. Here, the equation reported by Li and Zhang, who calculate on the base of Pike and Seager's equation, is used to get the critical density ay the percolation limit: [21]

$$n_c = \frac{5.63726}{l^2} \tag{5.1}$$

,which refers to the relationship for the critical number density of nanowire required for percolation limit (n_c) at a fixed length. Figure 5.14 also shows the idea of percolation limit for 2-D nanowire network. The equation indicated that longer nanowires can exhibit higher transparency TCOs because the number required for percolation limit is lower.

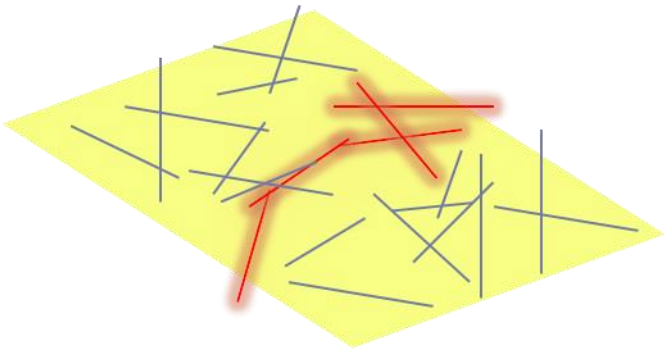

Figure 5.14. Percolation for random nanowire network

Both equation and the simulation result indicated that longer nanowires can exhibit higher transparency TCOs because the number required for percolation limit is lower.

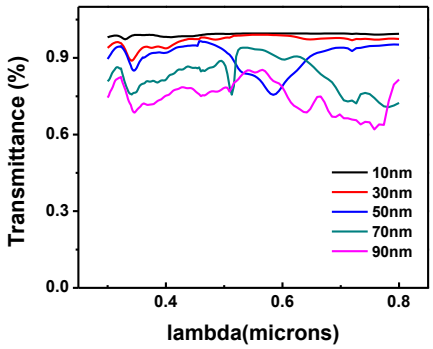

Figure 5.15. The transmittance for nanowire networks with different diameters at percolation limit

5.3.4 Percolation limit and conductance relationship

In discussing the effect of percolation limit with performance of transparent and conducting film, we can not only pay attention on the transmittance. In fact, the percolation limit also shows the electron transfer behavior throughout the film thus is critical for explanation of the electrical conductance. [21]

$$\sigma \propto (N-N_c)^{\Upsilon} \tag{5.2}$$

, where Υ is the conductance exponent, theoretically =4/3 for 2-D network when $N < 2N_c$. For thinner nanowires, the total density N is larger, but the critical density N_c is smaller. As a result, the conductance and transmittance are more preferred.

However, the previous discussion is focus on the percolation limit when the links between nanowires matters. When the silver concentration is high enough that silver nanowires are well linked to each other, $N >> N_c$, it not a percolation limit problem anymore. This explanation is not valid for the nanowire networks that are highly connected. The random sizes of hole created by the nanowire network, the junction of nanowires, the electrons emitted into nearby TCOs and other factors may lead to different conclusion when the silver concentration is high. From our experimental results, the longer and thicker nanowires show a better performance when the density of nanowires exceeds the percolation limitation.

5.4 TRANSMITTANCE IMPROVEMENT BY SILVER NANOPARTICLES

5.4.1 Characterization of nanoparticles

In this section, we want to discuss the possibility that small silver nanoparticles can decorate on nanowire and improve the transmission as a result. Silver nanoparticles we synthesized are tiny thus TEM is used to characterize the size of nanoparticles. From the figure 5.16, the size is around 20-50nm.

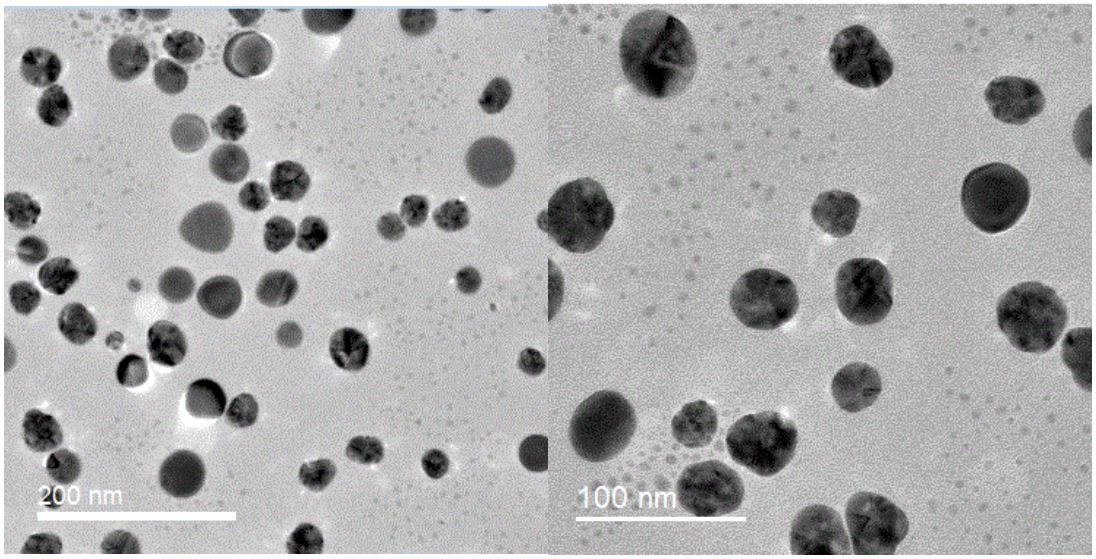

Figure 5.16. TEM for nanoparticles

5.4.2 Silver nanowire and nanoparticle mixture

In the fact that we use polyol method to synthesize the silver nanoparticles and nanowires, the PVP is stick on the surface of nanowires and nanoparticles. For the viscosity for PVP is much

higher than the TCO solution and the bond between PVP and silver, Ag^0-PVP, is strong, the nanoparticles tend to attach on the surface of nanowires with a certain gap because the ligand C-N and C=O give more electron density for sp orbital for Ag. We assume the tiny gap can be adjusted by the cleaning step using Acetone. Finally, after annealing, the PVP is totally removed, which leaves a gap between nanoparticles and nanowires.

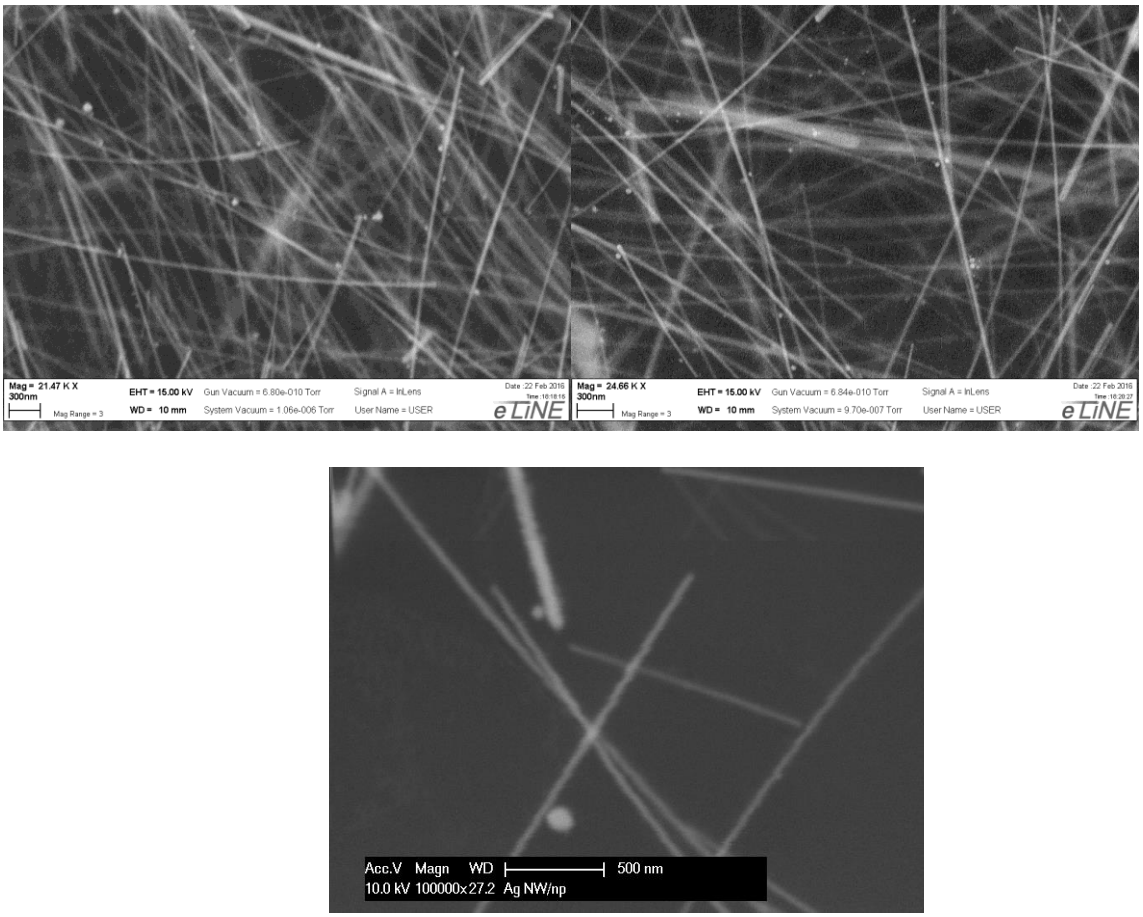

Figure 5.17. SEM of nanoparticle decorated nanowire

5.4.3 The effect on haze

Another possible explanation for the decoration of nanoparticles is Haze .Due to the rough surface of nanowire networks, the haze for pure nanowire network TCOs are really high. Nanoparticles may be a good helper to flat the surface and reduce the haze.

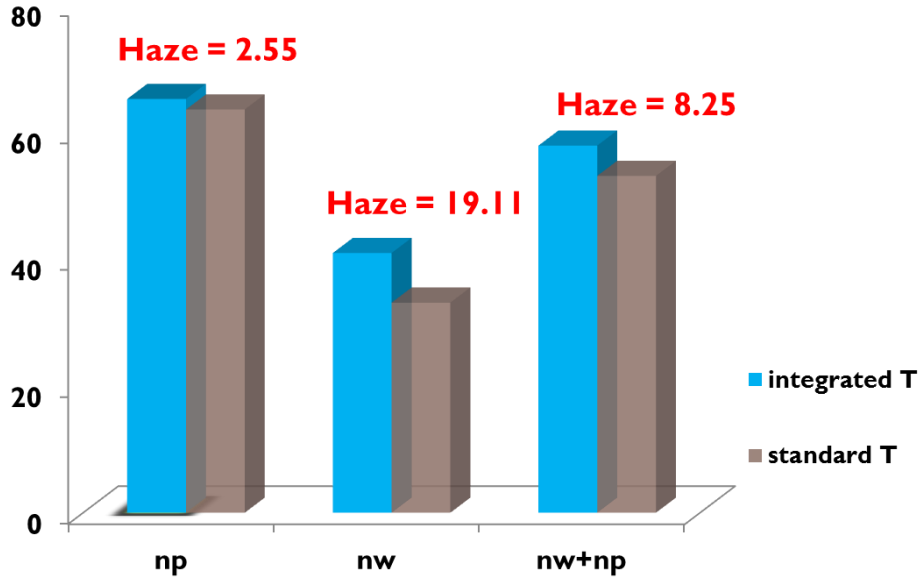

Figure 5.18. The comparison between integrated transmittance and standard transmittance for nanoparticles, nanowires and nanoparticle/nanowire mixture

For the calculation of Haze:

$$\text{Haze} = \frac{T_{diffusive}}{T_{total}} \% \tag{5.3}$$

Actually, the integrated transmittance measures both diffusive and specular transmittance, the standard transmittance measures only specular transmittance. From the Figure

5.18, it is clearly showed that the Haze is reduced from 19 to 8 by mixing nanoparticles into nanowires.

5.4.4 Mie scattering simulation

In order to further describe the effect of silver nanoparticles on silver nanowire. Here, we also do the optical simulation. The model is a simple silver nanowire with 5μm long and 30nm radius. One case is for the Mie scattering calculation for only nanowire. And the other case is the Mie scattering calculation for that nanowire decorated by several small silver nanoparticles with 10nm in radius.

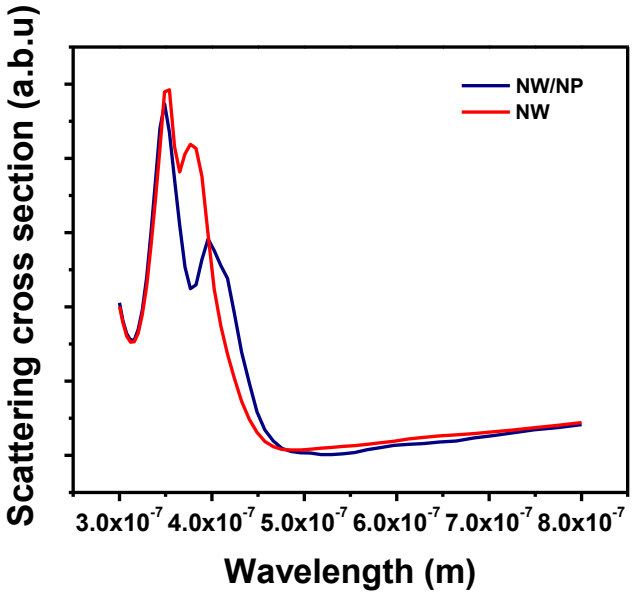

Figure 5.19 Mie scattering for a nanowire and a nanowire decorated with nanoparticles

5.4.5 The effect on FOM

In discussing the performance of TCOs, we still need to plot the figure of merit to verify the transmission and conductivity of our samples. From the Figure.5.19, the black line, which presenting Ag NW/NP mixture, has a higher transmittance but similar resistivity when the silver concentration is high.

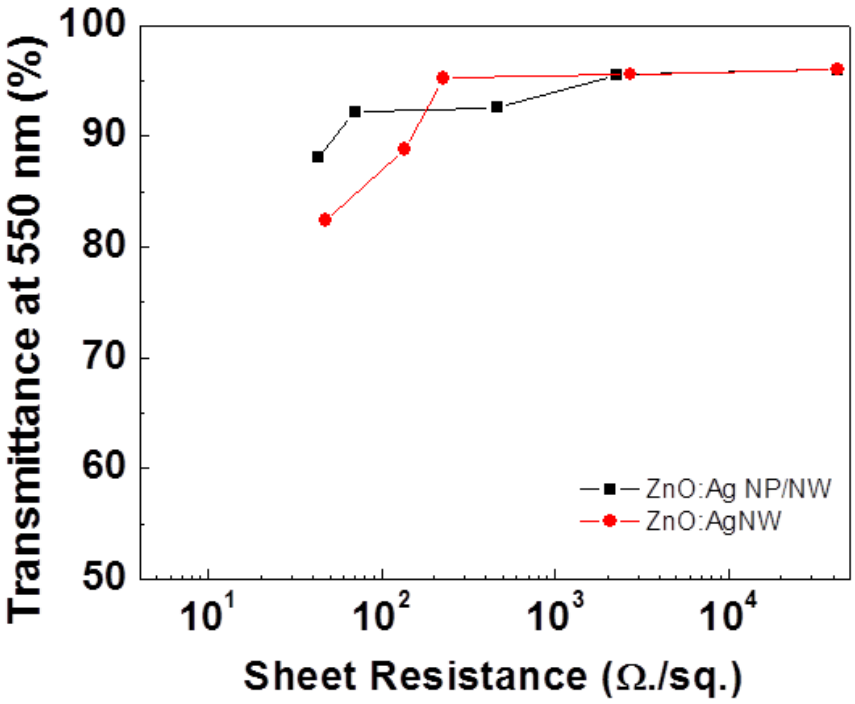

Figure 5.20. FOM of NW/NP mixture and NW

5.5 PEROVSKITE SOLAR CELL

TCOs can be widely used in different kinds of applications such as thin film solar cell productions. In this part, the perosvkite solar cell is introduced as the example of TCOs-related application.

Perovskite solar cell gets the name by its crystal structure ABX_3, which is called as perovskite crystal structure. The unit cell sketch is showed in Figure 2.2, where A = Cs, CH_3NH_3, $NH_2CH{=}NH_2$,

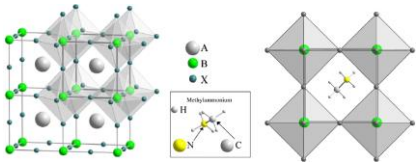

Figure 5.21. **Unit cell of ABX_3 perovskite solar cell**

For our future work, we want to apply the TCOs into a perovskite solar cell. The structure illustrated like Figure 5.21. ZnO layers serve as the blocking layers.

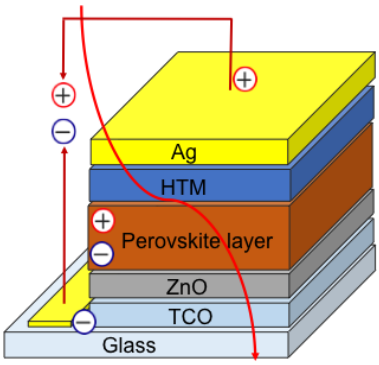

Figure 5.22. The perovskite solar cell structure

6.0 CONCLUSION

This study provided the discussion and explanation of random silver nanowire networks embedded AZO from both experimental aspect and simulating aspect. Electron transfer behaviors and optical properties are studied based on the Hall resistivity, mobility, carrier concentration, figure of merit and optical simulations.

Here, polyol method is applied to control the length and diameter of silver nanowires due to the temperature-dependence reducing power of polyol chemicals. Lower temperature inhibits the reducing ability of ethylene glycol thus slow down the silver nucleation rate. As a result, the nanowires produced under lower temperature tend to grow longer than the nanowires produced under higher temperature. Another observation is longer reaction time leads to longer and thicker nanowires. But if the reaction time is too long, silver nanowires length and diameter would decay until changing into small nanoparticles.

Then the random silver nanowire networks are embedded into AZO in order to improve the electrical conductivity of TCO films at the same time not affect the optical transparency too much. The Hall resistivity is dramatically decreased with the increasing silver concentration, while the Hall mobility and Hall carrier concentration are enhanced compared to the pure AZO. For better evaluation the performance of silver nanowire network embedded AZO, we plot the figure of merit. It shows that the transmittance of films is over than 80% with a best resistivity around 15Ωcm. The performance is as good as the “Gold Standard” TCOs.

Further discussion using FDTD simulation is shown in order to study the silver nanowire networks under percolation limit. When the concentration of silver nanowires is less than two times of percolation limit, the connectivity of silver nanowires is critical. Thinner nanowires lead to higher transmittance and higher conductivity. As a result, under percolation limit, the thinner and longer nanowire network is preferred. However, when the concentration of silver nanowires increases, the nanowires can connect well with each other. The lengths of nanowires influence the conductivity and transmittance. Experimentally, when the silver nanowire concentration is higher, thicker and longer nanowire networks can also have better performance according to the figure of merit.

Finally, the discussion about silver nanoparticles decorated nanowires is provided. According to the SEM images, the silver nanoparticles tend to locate on the surface of nanowires with a small gap. A possible explanation is that the silver nanowires and nanoparticles are synthesized using polyol method. The surfactant PVP can build up a bond with silver. After embedded the silver into AZO and annealing at 500°C, the PVP is totally removed leaving the small gaps between silver nanowires and nanoparticles, which may be helpful to increase the transmittance and reduce the haze causing by the rough surfaces produced by nanowire networks.

BIBLIOGRAPHY

[1]"ZnO - An Advanced Material for Solar Cell, Optoelectronic and Sensor Applications." - *Springer*. N.p., n.d. Web. 28 Mar. 2016.

[2]"Transparent Conducting Oxides-An Up-To-Date Overview." *ResearchGate*. N.p., n.d. Web. 28 Mar. 2016.

[3]"New N-Type Transparent Conducting Oxides." *ResearchGate*. N.p., n.d. Web. 28 Mar. 2016.

[4]"Preparation of Aluminum Doped Zinc Oxide Films and the Study of Their Microstructure, Electrical and Optical Properties." *Preparation of Aluminum Doped Zinc Oxide Films and the Study of Their Microstructure, Electrical and Optical Properties*. N.p., n.d. Web. 28 Mar. 2016.

[5]"Low Temperature Synthesis of Sol–gel Derived Al-doped ZnO Thin Films with Rapid Thermal Annealing Process." - *Springer*. N.p., n.d. Web. 28 Mar. 2016.

[6]"Hydrogen as a Cause of Doping in Zinc Oxide." *Physical Review Letters*. N.p., 31 July 2000. Web. 28 Mar. 2016.

[7]32, Ieee Eds Mini-Colloquium Wimnact. *ZnO-based Transparent Conductive Oxide Thin Films* (n.d.): n. pag. Web.

[8]"Chemical Society Reviews." *Size Matters: Why Nanomaterials Are Different - (RSC Publishing)*. N.p., n.d. Web. 28 Mar. 2016.

[9]"Electronic Structure of P-type Conducting Transparent Oxides." *Electronic Structure of P-type Conducting Transparent Oxides*. N.p., n.d. Web. 28 Mar. 2016.

[10]"Formation of PVP-Protected Metal Nanoparticles in DMF." *ResearchGate*. N.p., n.d. Web. 28 Mar. 2016.

[11]"Fused Silver Nanowires with Metal Oxide Nanoparticles and Organic Polymers for Highly Transparent Conductors." - *ACS Nano (ACS Publications)*. N.p., n.d. Web. 28 Mar. 2016.

[12]"Highly Robust Indium-Free Transparent Conductive Electrodes Based on Composites of Silver Nanowires and Conductive Metal Oxides." - *Zilberberg*. N.p., n.d. Web. 28 Mar. 2016.

[13]"Improvement of Transparent Conducting Materials by Metallic Grids on Transparent Conductive Oxides." *Improvement of Transparent Conducting Materials by Metallic Grids on Transparent Conductive Oxides*. N.p., n.d. Web. 28 Mar. 2016.

[14]"Nanoparticle-Mediated Coupling of Light into a Nanowire." *Nanoparticle-Mediated Coupling of Light into a Nanowire*. N.p., n.d. Web. 28 Mar. 2016.

[15] *Nature.com*. Nature Publishing Group, n.d. Web. 28 Mar. 2016.

[16]Xie, Shouyi, Zi Ouyang, Nicholas Stokes, Baohua Jia, and Min Gu. "Enhancing the Optical Transmittance by Using Circular Silver Nanowire Networks." *J. Appl. Phys. Journal of Applied Physics* 115.19 (2014): 193102. Web.

[17]"Preprint of Phys. Rev. Lett. 88, 095501 (2002)." *ResearchGate*. N.p., n.d. Web. 28 Mar. 2016.

[18]"Publication Citation: Integrating Sphere Method for Absolute Transmittance, Reflectance and Absorptance of Specular Samples." *NIST Manuscript Publication Search*. N.p., n.d. Web. 28 Mar. 2016.

[17]"Shape and Size Dependence of Radiative, Non-radiative and Photothermal Properties of Gold Nanocrystals." *Shape and Size Dependence of Radiative, Non-radiative and Photothermal Properties of Gold Nanocrystals*. N.p., n.d. Web. 28 Mar. 2016.

[19]Tvarozek, Vladimir, Pavol Sutta, Sona Flickyngerova, Ivan Novotny, Pavol Gaspierik, Marie Netrvalova, and Erik Vavrinsky. "Preparation of Transparent Conductive AZO Thin Films for Solar Cells." *Semiconductor Technologies* (2010): n. pag. Web.

[20]"Chapter 11." *Silver Nanoparticles: Sensing and Imaging Applications*. N.p., n.d. Web. 28 Mar. 2016.

[21]1. *PERCOLATION THEORY AND NETWORK MODELING APPLICATIONS IN SOIL PHYSICS* (n.d.): n. pag. Web.

[22]"Study of Transparent Indium Tin Oxide for Novel Optoelectronic Devices." - *OpenGrey*. N.p., n.d. Web. 28 Mar. 2016.

[23]"Liquid Phase Methanol and Dimethyl Ether Synthesis from Syngas." - *Springer*. N.p., n.d. Web. 28 Mar. 2016.

[24]"Synthesis of Aqueous Gold Nanoparticles." *Chem553project* -. N.p., n.d. Web. 28 Mar. 2016.

[25]006. *Rayleigh, Mie, and Optical Scattering* (n.d.): n. pag. Web.

[26]"Microwave-driven Synthesis of Iron Oxide Nanoparticles for Fast Detection of Atherosclerosis | Protocol." *Microwave-driven Synthesis of Iron Oxide Nanoparticles for Fast Detection of Atherosclerosis | Protocol*. N.p., n.d. Web. 28 Mar. 2016.

[27]"Surfactant Free, Non-aqueous Method, for the Deposition of ZnO Nanoparticle Thin Films on Si(100) Substrate with Tunable Ultraviolet (UV) Emission." *Http://www.eurekaselect.com*. N.p., n.d. Web. 28 Mar. 2016.

[28]"Surface Plasmon Resonance Sensors: Review." *Surface Plasmon Resonance Sensors: Review*. N.p., n.d. Web. 28 Mar. 2016.

[29]"4. Metal Oxide Nanoparticles." *Nanoparticles* (n.d.): n. pag. Web.

[30]Cushing, Brian L., Vladimir L. Kolesnichenko, and Charles J. O'connor. "Recent Advances in the Liquid-Phase Syntheses of Inorganic Nanoparticles." *Chemical Reviews Chem. Rev.* 104.9 (2004): 3893-946. Web.

[31]"Intrinsic Limitations to the Doping of Wide-gap Semiconductors." *Intrinsic Limitations to the Doping of Wide-gap Semiconductors*. N.p., n.d. Web. 28 Mar. 2016.

[32]"Sheet Resistance and the Calculation of Resistivity or Thickness Relative to Semiconductor Applications." *Four Point Probes*. N.p., 15 May 2013. Web. 28 Mar. 2016.

[33]"Patent US6559941 - UV-VIS Spectrophotometry." *Google Books*. N.p., n.d. Web. 28 Mar. 2016.

[34]"Poly(vinyl Pyrrolidone)-capped Five-fold Twinned Gold Particles with Sizes from." *Poly(vinyl Pyrrolidone)-capped Five-fold Twinned Gold Particles with Sizes from*. N.p., n.d. Web. 28 Mar. 2016.